

1 **Microbial strong organic ligand production is tightly coupled to iron in** 2 **hydrothermal plumes**

3
4 Colleen L. Hoffman^{1,2,3*†} and Patrick J. Monreal^{3,4*†}, Justine B. Albers⁵, Alastair J.M. Lough⁶, Alyson E.
5 Santoro⁵, Travis Mellett^{3,7}, Kristen N. Buck^{7,8}, Alessandro Tagliabue⁹, Maeve C. Lohan⁶, Joseph A.
6 Resing^{1,2,3}, Randelle M. Bundy³

7
8 ¹Joint Institute for the Study of Atmosphere and Ocean, University of Washington, 3737 Brooklyn
9 Avenue NE, Seattle, WA 98195, USA

10 ²Cooperative Institute for Climate, Ocean, and Ecosystem Studies, University of Washington,
11 3737 Brooklyn Avenue NE, Seattle, WA 98195, USA

12 ³School of Oceanography, University of Washington, 1501 NE Boat Street, Seattle, WA 98195,
13 USA

14 ⁴Earth Systems Program, Stanford University, 473 Via Ortega, Stanford, CA 94305,
15 USA

16 ⁵Department of Ecology, Evolution, and Marine Biology, University of California, Santa Barbara,
17 CA 93106, USA

18 ⁶Department of Ocean and Earth Sciences, National Oceanography Centre, University of
19 Southampton, European Way, Southampton SO14 3ZH, United Kingdom

20 ⁷College of Marine Science, University of South Florida, 140 7th Avenue South, St. Petersburg,
21 FL, 33701, USA

22 ⁸College of Earth, Oceans, and Atmospheric Sciences, Oregon State University, 2651 SW Orchard Ave,
23 Corvallis, OR, 97331, USA

24 ⁹Department of Earth, Ocean, and Ecological Sciences, University of Liverpool, 4 Brownlow
25 Street, Liverpool l69 3GP, United Kingdom

26
27 †These authors contributed equally and ~~should be considered~~are co-first authors

28 *Correspondence: Colleen L. Hoffman and Patrick J. Monreal

29 **Email:** clhoffma@gmail.com, pmonreal@uw.edu

30

31

32

33

34 **Abstract.** Hydrothermal vents have emerged as ~~an~~ important sources of iron to seawater, yet only a subset
35 of this iron is soluble and persists long enough to impact the deep ocean iron inventory. The longevity and
36 solubility of iron in seawater is in part governed by strong organic ligands, like siderophores, that are
37 produced by microorganisms and are a part of the ocean's dissolved organic iron-binding ligand pool. These
38 ligands have been hypothesized to aid in the persistence of dissolved iron in hydrothermal environments. To
39 explore this hypothesis, we measured iron and iron-binding ligands including siderophores from 11
40 geochemically distinct sites along a 1,700 km section of the Mid-Atlantic Ridge. Siderophores were found
41 in hydrothermal plumes at all sites, with proximity to the vent playing an important role in dictating
42 siderophore type and diversity. The notable presence of amphiphilic siderophores may point to microbial
43 utilization of siderophores to access particulate hydrothermal iron, and the exchange of dissolved and
44 particulate iron. The tight coupling between strong ligands and dissolved iron within neutrally buoyant
45 plumes across distinct hydrothermal environments, and the presence of dissolved siderophores with
46 siderophore-producing microbial genera, suggests that biological production of ligands ~~exerts a key~~
47 ~~control~~ influence iron chemistry on in hydrothermal ~~dissolved iron concentrations~~ systems.

48 1. Introduction

49 Over the last few decades, observations and modelling efforts have increased our understanding about the
50 critical role ~~organic~~ organic ligands play in the cycling, transport, and utilization of trace metals in deep water
51 (Tagliabue et al., 2017; Buck et al., 2018; Bundy et al., 2018; Moore et al., 2021; Hawkes et al., 2013b; Kleint
52 et al., 2016). Iron (Fe) binding organic ligands in deep seawater have a wide range of sources, which are only
53 just beginning to be understood. Recent observations suggest that microbial production of siderophores,
54 humic-like substances and exopolysaccharides are some of the major contributors of marine organic ligands
55 (Hassler et al., 2017), and ~~links~~ microbial activity production and alteration of ligands ~~to~~ influences Fe cycling
56 in environments ranging from hydrothermal plumes (Cowen and Bruland, 1985; Cowen et al., 1990) to the
57 open ocean (Lauderdale et al., 2020; Whitby et al., 2024, 2020; Misumi et al., 2013). Strong Fe-binding
58 organic ligands (defined as L_1 ligands) are a heterogeneous mixture of microbially produced compounds that
59 are operationally classified based on their binding strength with Fe (defined as $\log K_{Fe', FeL}^{cond} > 12$). They are
60 thermodynamically favored to complex and stabilize external sources of Fe to prevent its scavenging and
61 removal (Fishwick et al., 2014; Aguilar-Islas et al., 2010). As an example, in high Fe estuarine systems, only
62 the dissolved Fe (dFe) bound to the strongest Fe-binding ligands is protected from scavenging and remains
63 in solution (Bundy et al., 2015; Buck et al., 2007).

64
65 Siderophores are the strongest known Fe-binding organic ligands. They are produced by bacteria and fungi
66 to facilitate Fe uptake and solubilize otherwise inaccessible phases in the marine environment (Butler, 2005;
67 Manck et al., 2022). They have primarily been considered an important microbial strategy for Fe acquisition
68 in the low dissolved Fe (dFe) < 0.5 nM surface ocean (Vraspir and Butler, 2009; Butler, 2005). However,

69 siderophore uptake and biosynthesis genes were observed in >70% of Fe-related bacterial transcripts in a
70 hydrothermal environment in Guaymas Basin (Li et al., 2014), have been identified in oxygen-deficient zones
71 (Moore et al., 2021), and are a common Fe acquisition strategy within terrestrial and pathogenic ecosystems
72 (Sandy and Butler, 2009), all of which are environments where Fe concentrations are orders of magnitude
73 higher than surface seawater.

74

75 Previous studies have ~~both looked at examined~~ unknown ~~strong~~-Fe-binding ligands ~~besides siderophores~~ in
76 hydrothermal plumes and throughout the deep ocean (Buck et al., 2018; Kleint et al., 2016; Hawkes et al.,
77 2013b; Sander and Koschinsky, 2011), as well as siderophores observed below the euphotic zone (Bundy et
78 al., 2018; Park et al., 2023a; Moore et al., 2021; Boiteau et al., 2019). However, no previous studies have
79 ever directly measured siderophores in hydrothermal systems due to the high sample volume requirements,
80 difficulty in obtaining deep ocean trace metal samples, and the time-intensive nature of the analyses. A
81 ‘stabilizing agent’ (i.e. ligands) has been proposed for the long-range transport of hydrothermal dFe into the
82 ocean interior. The role of strong Fe-binding ligands in hydrothermal dFe transport represents an important
83 knowledge gap in how hydrothermal vents may impact the ocean dFe inventory (Resing et al., 2015) and
84 how siderophores may influence Fe transformations in hydrothermal systems. Here, for the first time, we
85 identified siderophores and siderophore-producing microbes in 11 geochemically distinct hydrothermal
86 environments along the slow-spreading (20-50 mm/yr) Mid-Atlantic Ridge (MAR). Four black smokers
87 (high temperature, high Fe), four off-axis sites, one diffuse vent (low temperature, low Fe), one alkaline vent
88 (pH 9-11, very low Fe), and one non-vent fracture zone were investigated using both competitive ligand
89 exchange-adsorptive cathodic stripping voltammetry and state-of-the-art liquid chromatography coupled to
90 electrospray ionization mass spectroscopy (Boiteau et al., 2016) in a targeted approach to search for known
91 siderophores identify and possible discrete compound components of present in the L₁ ligand pool in
92 hydrothermal environments and to search for known siderophores. Microbial community analysis was also
93 compared at three sites to understand whether microbial ligand production impacts Fe transformation the
94 supply of in hydrothermal dFe to the oceans systems. Overall, our results show microbially-produced
95 siderophores were present in all sites, and that strong L₁ ligands were tightly coupled to hydrothermal dFe
96 concentrations in the neutrally-buoyant plume samples in this system. The presence of organic ligands
97 produced by bacteria in hydrothermal systems suggest that they play an important role in deep ocean Fe
98 cycling.

99 2. Results and Discussion

100 2.1 The role of iron-binding ligands in hydrothermal plumes

101 Strong ~~organic~~-Fe-binding ligands (~~defined here as~~-L₁ ligands) have ~~been previously been~~ found ~~to be~~
102 ~~important~~ in neutrally-buoyant hydrothermal plumes across a variety of systems (Tagliabue et al., 2017;
103 Resing et al., 2015; Buck et al., 2018; Hawkes et al., 2013b; Wang et al., 2022; Bennett et al., 2008). ~~But~~
104 However, the relationship between organic ligands and dFe have never been investigated together

105 systematically across a wide variety of vents in the same study. In this work, the average binding strength
106 and concentration of organic Fe-binding ligands were quantified in 11 vent systems that spanned a wide range
107 in dFe concentrations (0.41-90 nM) and underlying vent geology. Over 99% of dFe in the neutrally buoyant
108 plume ~~samples~~ were complexed by L₁ ligands and the ligands were almost always completely saturated with
109 dFe, meaning Fe-free ‘excess’ L₁ ligands capable of binding additional Fe were present in low concentrations
110 (< 1 nM; **Fig. S1**). As a result, dFe concentrations were tightly coupled to L₁ ligands in a nearly 1:1 ratio
111 (**Fig. 1d**), similar to previous studies in other neutrally buoyant plumes (**Fig. 1e**) (Lough et al., 2022; Buck
112 et al., 2018, 2015).

113 The strong coupling between dFe and ligands was only observed at sites where L₁ ligands were detected.
114 Some ~~samples~~ ~~locations, such as in the~~ ~~that were closer to the~~ buoyant plume ~~and vent source~~ ~~or closer to~~
115 ~~the vent orifice~~, contained high concentrations of weaker ligands ($\log K_{Fe,FeL}^{cond} < 12$, **Table S2-S3**) ~~with whose~~
116 ~~concentrations had~~ no correlation ~~to~~ ~~with~~ dFe. This is consistent with these environments likely being
117 dominated by ~~complex Fe phases, which could include various~~ inorganic forms (e.g. ~~nanopyrite, Fe-~~
118 ~~oxyhydroxide~~) ~~of Fe as well as mixed organic phases of Fe~~ as hydrothermal fluids initially mix with
119 oxygenated seawater. ~~High concentrations of weaker ligands have also been observed in samples near the~~
120 ~~vent orifice in previous studies (Hawkes et al., 2013). In this study, we are not able to discern the exact~~
121 ~~chemical composition of the ligands we detect via voltammetric methods, and thus the weaker and some~~
122 ~~portion of the stronger ligands we observe likely represent a mix of different inorganic and organic ligands.~~
123 ~~Similar to what was described in Hawkes et al. (2013), the ligands we measure could represent multiple~~
124 ~~layers of coordination bonds, forming complex Fe phases, similar to the “onion” concept~~ (Mackey
125 and Zirino, 1994). ~~For example, colloidal Fe phases are common in hydrothermal vents and can form~~
126 ~~aggregates that bind Fe, but not in traditional organic coordination bonds~~ (Fitzsimmons et al., 2017;
127 Honeyman and Santschi, 1989). ~~There are also likely processes occurring near the vent source in such a~~
128 ~~complex environment that cause some Fe phases to be in various stages of disequilibria that we also measure~~
129 ~~as ligands via our voltammetric methods.~~

130
131 ~~The sources of~~ ~~Moreover, weaker~~ Fe-binding ligands ~~with a~~ ($-\log K_{Fe,FeL}^{cond} < 12$) ~~that have been observed in~~
132 ~~other hydrothermal systems globally, and yet their role in Fe cycling in these environments is not well~~
133 ~~understood, and their impact on Fe cycling over the lifetime of neutrally-buoyant plume is unclear. Recent~~
134 ~~studies have shown microbes may use siderophores or siderophore-like (strong binding ligands) ligands to~~
135 ~~access the iron~~ Fe associated with weaker ~~type~~ ligands — such as humic substances and thiols — ~~and to~~
136 ~~enhance the cycling and bioavailability of Fe in aquatic systems~~ (Kuhn et al., 2014; Muller, 2018). However,
137 ~~to date, only the few studies that have explored ligands concentrations and binding strengths within~~
138 ~~hydrothermal systems~~ (Buck et al., 2015, 2018; Kleint et al., 2016; Hawkes et al., 2013c; Sander and
139 Koschinsky, 2011) ~~and they have mixed results~~ ~~hypotheses~~ as to the role and sources of weaker-type ligands
140 ~~within plumes. Additional studies are needed to investigate the sources and mechanisms of weaker-type~~
141 ~~ligands in hydrothermal plumes and understand their impact on the Fe cycle in hydrothermal systems.~~

142

143

144 ~~In the neutrally buoyant plume samples. Overall, our voltammetry results indicate that stronger~~ L₁ ligands
145 ~~were present and were eap-correlated with~~ the dFe concentrations ~~in neutrally-buoyant plumes~~(Fig. 1) and
146 ~~weaker ligands were no longer dominant. In other systems with a high dFe and ligand endmember such as~~
147 ~~estuaries, a decrease in weaker ligands along with dFe concentrations has also been observed (Buck et al.,~~
148 ~~2007; Bundy et al., 2014). This has been interpreted as a scavenging of weaker Fe-ligand complexes, while~~
149 ~~the dFe that remains in solution is that which is bound to stronger ligands (Bundy et al., 2014). A similar~~
150 ~~control on dFe concentrations by L₁ ligands has also been previously observed in estuaries (Buck et al., 2007)~~
151 ~~and aerosol solubility experiments (Fishwick et al., 2014). There are a few possible explanations for the~~
152 ~~correlation of dFe and L₁ ligands in the neutrally-buoyant plume.~~ One possible explanation is that both the
153 dFe and L₁ ligands originate from the vent fluids themselves, yielding a tightly coupled hydrothermal
154 endmember. However, the concentration of L₁ ligands did not correlate with excess mantle Helium-3 (³He_{xs},
155 **Fig S2, Table S2-S3**) (Lough et al., 2022), a nearly conservative tracer of the mixing of hydrothermal fluids
156 with seawater (Buck et al., 2018), ~~and Moreover,~~ our samples closer to the vent source were dominated by
157 weaker organic ligands showing no correlation to dFe. This suggests the L₁ ligands were not directly sourced
158 from the vent fluids along with dFe. ~~Biological sources represent a~~Another likely explanation is the source for
159 ~~the coupling~~ of L₁ ligands ~~and dFe, if the ligands~~ observed in the neutrally-buoyant plume are ~~either~~ from
160 bacteria that produced them in surrounding deep ocean seawater that was then entrained, local production
161 from vent-biota and/or microbial mats, diffusion from microbial production in sediments, or *in-situ*
162 production by bacteria within the neutrally buoyant plume (Mellett et al., *submitted*)(Dick et al., 2013; Li et
163 al., 2014; Sheik et al., 2015; Mellett et al., *submitted*n.d.). ~~Previous work has shown the genetic potential for~~
164 ~~plume associated microbial populations to produce siderophores (Li et al., 2014)~~

165

166 2.2 The presence of siderophores in hydrothermal systems

167 Siderophores were measured in a subset of the samples to further explore the source of the L₁ ligands coupled
168 to dFe in the neutrally-buoyant plume. Marine organic ligand composition changes with environmental
169 gradients (Boiteau et al., 2016; Gledhill and Buck, 2012), making the structure and functional groups of
170 siderophores identified in hydrothermal samples of particular interest. Somewhat surprisingly, siderophores
171 were found in all samples and we observed a large diversity of siderophores with high confidence using mass-
172 to-charge ratio (*m/z*), MS/MS spectra, and specific chromatographic characteristics (**Fig. 2a**). On-axis
173 spreading centers contained the highest dFe concentrations (> 20 nM) and wider variety of siderophores than
174 samples from fracture zones, diffuse, and off-axis sites (dFe ≤ 1 nM). The greatest number of distinct
175 siderophores were identified at Lucky Strike, Broken Spur, Rainbow, and TAG (**Fig. 2**). On average, 13
176 compounds were identified with high confidence per on-axis spreading center sample, compared with 5 per
177 diffuse/fracture zone sample, and 2.5 per off-axis sample (**Fig. 2b, Fig. S4**). Mixed-type siderophores —

178 containing different moieties that bind to Fe(III) — were common at all sites. Hydroxamates were identified
179 at and around spreading centers, yet none of these were detected with high confidence in samples from
180 diffuse/fracture zones (**Fig. S4**). Summed siderophore abundance in neutrally-buoyant plumes above
181 spreading centers was similarly more than twice that of samples from fracture zones or off-axis (**Fig. 2c**).
182 Thus, vent type and proximity played a role in the diversity and abundance of siderophore types observed,
183 likely related to the diversity of the microbial community and/or unique Fe acquisition strategies across sites.
184

185 Siderophores are ~~putatively operationally~~ part of the operational L₁ ligand pool based on their binding
186 strength (Gledhill and Buck, 2012), and patterns in their distributions ~~reflected-were similar to~~ those of the
187 strong ligands. The peak areas of each putative siderophore we identified were used as a proxy for
188 concentrations (*section 3.3*), and these concentrations significantly correlated with dFe, as observed with dFe
189 and L₁ ligands (**Fig. 2b**). Siderophores were present in concentrations similar to the surface ocean (Boiteau
190 et al., 2016; Moore et al., 2021; Park et al., 2022; Bundy et al., 2018), and ~~comprised-were equivalent to~~
191 concentrations representing 0.01-0.4% of the total L₁ ligands (**Table 1**). This is ~~likely~~ a substantial
192 underestimate of siderophore contributions to the L₁ ligand pool due to analytical constraints in identifying
193 unknown siderophores. Recent work on siderophore biosynthesis pathways and advances in genome mining
194 suggest that known siderophores represent a small fraction of what is expected to be produced in nature
195 (Hider and Kong, 2010; Reitz et al., 2022), and our analyses in this study were limited to only known
196 siderophores. We also restricted our reporting to compounds identified with very high confidence (Fig 2a,
197 S3). In addition, most siderophores are not commercially available to use as standards, and individual
198 siderophores have different ionization or extraction efficiencies. ~~We restricted our reporting to compounds~~
199 ~~only identified with very high confidence (Fig 2a, S3).~~ The extraction efficiency for the solid phase extraction
200 technique is approximately 5-10% for bulk Fe-binding organics (Bundy et al., 2018) and 40% for a
201 siderophore standard (Waska et al., 2015). Employing both corrections yields siderophore contributions to
202 the total L₁ pool of 0.1-4% and 0.025-1%, respectively. We are inevitably missing many naturally occurring
203 unknown compounds, and thus we consider this a lower bound. Regardless of the small percentage
204 contribution to total L₁ ligands, it is evident that microbially produced siderophores were ubiquitous across
205 all vent sites and had similar distributional patterns as L₁ ligands. There are also likely other compounds such
206 as some strong binding humics that are also contributing to the L₁ ligand pool (Laglera and van den Berg,
207 2009). Future work with much larger water volumes will be able to reduce uncertainty and identify a greater
208 number of compounds. Still, ~~t~~The identification of siderophores here — and their relationship with dFe —

209 provides compelling evidence that microbial production of ligands is responsible for at least some portion of
210 the tight coupling between L₁ and dFe in hydrothermal systems along the MAR.

211

212 The presence and diversity of siderophores identified in this system was surprising given the relatively high
213 Fe concentrations of hydrothermal environments, but some ~~interesting-compelling~~ patterns were observed.
214 For example, previous work has shown that low Fe surface waters have higher concentrations of amphiphilic

215 siderophores compared to high Fe coastal waters (Boiteau et al., 2016), and amphiphilic siderophores are less
216 common in terrestrial environments (Hider and Kong, 2010). Amphiphilic siderophores have long
217 hydrocarbon tails that can be embedded into the lipid bilayer of the bacterial cell membrane providing a
218 mechanism to shuttle Fe into the cell and prevent diffusive loss (Martinez et al., 2003). Amphiphilic
219 siderophores comprised 57% of the siderophores in our samples (**Fig. S5**), supporting the ubiquity of
220 amphiphilic siderophores in marine environments (Butler and Theisen, 2010). Amphiphilic siderophores
221 were found in concentrations between 0.3-4.7 pM, with the highest concentrations found at Rainbow (**Fig.**
222 **2d, Table S6**). These concentrations were similar to those observed in the upper ocean (Boiteau et al., 2016;
223 Bundy et al., 2018; Boiteau et al., 2019). Marine bacteria produce suites of amphiphilic siderophores as a
224 way to adapt to the change in hydrophilicity in the surrounding environment (Sandy and Butler, 2009;
225 Homann et al., 2009). Amphiphilic siderophores in plumes could be a way for bacteria to access Fe as they
226 are physically transported and cope with strong chemical gradients, similar to the production of multiple
227 siderophores in terrestrial and pathogenetic systems as a means to access inorganic particulate Fe for cellular
228 uptake and storage (Hider and Kong, 2010).

229

230 **2.3 Microbial sources of siderophores in hydrothermal plumes**

231 The high diversity of siderophores across a huge range of hydrothermal vent systems revealed several
232 surprising aspects of Fe cycling. The biosynthesis of a siderophore is energy-intensive and is regulated by Fe
233 concentration in the surrounding environment (Rizzi et al., 2019). Siderophore presence suggests that bacteria
234 are producing these compounds despite the overall higher Fe concentrations in the deep ocean and within
235 hydrothermal plumes. Consistent with siderophore utilization in terrestrial ecosystems (Hider and Kong,
236 2010; Sandy and Butler, 2009), one hypothesis is that siderophore production is beneficial to bacteria in the
237 plumes for transforming Fe from otherwise inaccessible forms, such as particulate nanopyrites or Fe
238 oxyhydroxides that are present close to the vent source. To explore the potential for microbial production of
239 siderophores, we examined microbial community composition around Rainbow (St. 11, 17) and Lucky Strike
240 (St. 7; **Table 1, Table S1**) using 16S rRNA gene-based amplicon sequencing to detect bacteria with the
241 metabolic potential to synthesize siderophores (**Fig. 3, S11**), where the presence of taxa encoding siderophore
242 biosynthetic gene clusters indicates whether the microbial community is genetically capable of producing the
243 compounds we observed. Bacterial genera containing known siderophore-producers were found at all three
244 MAR sites examined, and putative siderophore-producers represented 3-20% of the relative abundance of
245 the community (**Fig. 3**). Putative siderophore-producers were more abundant in the 3 μm (particle-attached)
246 size fraction than in the 0.2 μm (free-living) fraction, suggesting siderophore production is more common in
247 particle-associated bacteria in hydrothermal environments.

248

249 We found microbial genera in our samples that can produce a subset of the siderophores identified here,
250 including ferrioxamines, vibrioferrin, and acinetoferrin (Butler, 2005; Vraspir and Butler, 2009; Moore et al.,

251 2021; Bundy et al., 2018; Boiteau et al., 2016). Genera with the genetic potential to produce ferrioxamines
252 were present at all three sites, while those known to produce vibrioferrin were present at Lucky Strike and
253 Rainbow, and those producing acinetoferrin were also present at Rainbow (**Table S1, S76**). Mycobactins
254 were detected with high confidence in every sample of this study, and genes encoding mycobactin have been
255 detected in a cultured organism from a hydrothermal system (Gu et al., 2019), but no mycobactin producers
256 were identified in this study. We detected woodybactin D with high confidence in 5 out of 11 sites. Although
257 these biosynthetic genes were not identified in any of the genera observed, woodybactin D is a carboxylate
258 siderophore isolated from *Shewanella* (Carmichael et al., 2019), and groups of deep-sea *Shewanella* (Kato
259 and Nogi, 2001) were found in the dataset (**Fig. S11**). The biosynthesis genes for many of the siderophores
260 identified are unknown. Thus, finding genera capable of producing only a subset of the siderophores
261 characterized is not surprising. The observation that a significant portion of the *in-situ* microbial community
262 is capable of synthesizing siderophores (**Fig 3**) suggests that siderophore production is more widespread in
263 the deep ocean than previously believed.

264

265 **2.4 The impact of strong ligands and siderophores on dissolved iron in neutrally-buoyant plumes**

266 Evidence that siderophores are ubiquitous in the marine environment — including higher Fe environments
267 — has been increasing (Park et al., 2023b). The high dFe associated with hydrothermal plumes may still not
268 be high enough to suppress siderophore production due to the elevated Fe requirements of heterotrophic
269 bacteria (Tortell et al., 1996). It is also likely that ~~in hydrothermal plumes~~ not all of the Fe is bio-accessible
270 ~~in hydrothermal plumes~~. Soil microbes secrete siderophores to solubilize particulate Fe (Crowley et al., 1991)
271 and similar processes could be occurring in hydrothermal plumes, where Fe mineral phases associated with
272 organic compounds are common (Hoffman et al., 2020; Toner et al., 2009; Fitzsimmons et al., 2017; Hoffman
273 et al., 2018; German and Seyfried, 2014; Holden et al., 2012). Although our measurements suggest that dFe
274 in the neutrally-buoyant plume is likely dominated by organic complexation, the L₁ measurements alone
275 cannot distinguish between purely organic phases or a mixture of inorganic and organic ligands in complex
276 aggregations or small colloids, as discussed above (section 2.1). Given the evidence from particulate Fe
277 studies in neutrally-buoyant plumes (Hoffman et al., 2020; Toner et al., 2009; Yücel et al., 2011; Fitzsimmons
278 et al., 2014, 2017; Hoffman et al., 2018)(~~Hoffman et al. 2020~~), it is highly likely that some portion of what
279 is detected in the L₁ pool is a mixture of organic and inorganic Fe in small colloids which are operationally
280 in the dFe pool (Fitzsimmons et al., 2017). It is also telling that most siderophore-producing genera were
281 found to be particle-associated (**Fig. 3**), providing additional evidence that siderophores might be produced
282 to solubilize particulate Fe or access other colloidal phases. Further work that assesses why bacteria are
283 producing siderophores in neutrally buoyant plumes will be important for understanding microbial
284 metabolism in these systems, and the impact of siderophore production on Fe dispersal.

285

286 Organic Fe-binding ligands have been implicated in playing a critical role in the preservation and transport
287 of hydrothermal dFe into the ocean interior (Hoffman et al., 2018; Resing et al., 2015; Fitzsimmons et al.,

288 2017; Toner et al., 2009; Bennett et al., 2011, 2008; Buck et al., 2018; Sander and Koschinsky, 2011). In this
289 work, L₁ ligands were tightly coupled to dFe in neutrally buoyant plumes along the MAR and the presence
290 of siderophores in these samples provided evidence for the first time, that at least some of these ligands are
291 microbially produced. How these complexes may facilitate the exchange of Fe between dissolved and
292 particulate phases (Fitzsimmons et al., 2017), and whether siderophores are present across additional
293 hydrothermal vent systems will aid in constraining the biogeochemical importance of microbial feedbacks in
294 impacting the hydrothermal dFe supply to the deep ocean.

295

296 **3. Appendix: Materials and Methods**

297 **3.1 Sampling and cruise transect**

298 Samples were collected as part of the 2017-2018 U.K. GEOTRACES GA13 section cruise along the Mid-
299 Atlantic Ridge. Water samples from 11 venting and near venting locations were collected using a Seabird
300 911 conductivity, temperature, and depth (CTD) titanium rosette using conducting Kevlar wire with an
301 oxidation-reduction potential (ORP) sensor to detect plumes. Teflon coated OTE (Ocean Test Equipment)
302 bottles were pressurized to approximately 7 psi with 0.2 µm filtered air using an oil free compressor. A
303 Sartobran 300 (Sartorius) filter capsule (0.2 µm) was used to collect filtered seawater samples into clean 250
304 mL LDPE sample bottles. Bottles and caps were rinsed 3 times with the filtered sample before being filled.
305 Samples were stored frozen at -20°C for Fe-organic ligand characterization by voltammetry and mass
306 spectrometry.

307 **3.2 Fe-binding ligand concentration and binding strengths Competitive Ligand Exchange-Adsorptive** 308 **Cathodic Stripping Voltammetry**

309 Fe-binding ligand concentrations and binding strengths (defined as conditional binding constants, $\log K_{Fe,FeL}^{cond}$
310 > 12) were determined by competitive ligand exchange-adsorptive cathodic stripping voltammetry (CLE-
311 ACSV) with a BASi controlled growth mercury electrode (CGME) with an Ag/AgCl⁻ reference electrode
312 and platinum auxiliary electrode (Bioanalytical Systems Incorporated). Using previously established
313 methods (Buck et al., 2015, 2018; Bundy et al., 2018; Abualhaija and van den Berg, 2014; Hawkes et al.,
314 2013c), 40 frozen filtrate (<0.2 µm) samples with dFe concentrations between 0.41-11.67 nM (**Table S1-**
315 **S2**) were thawed in a 4°C fridge prior to analysis. A 15-point titration curve was analyzed for each sample.
316 Briefly, within each titration, every point sequentially received 10 mL of sample, 7.5 mM of borate-
317 ammonium buffer, 10 µM salicylaldehyde (SA) added ligand, and a dFe addition. [Samples were then](#)
318 [equilibrated overnight before being measured on the BASi.](#)—Data was collected using the *Epsilon Eclipse*
319 *Electrochemical Analyzer* (v.213) with a deposition time of 120 seconds and analyzed using *ElectroChemical*
320 *Data Software* (v2001-2014) and *ProMCC* (v2008-2018) to determine peak areas and Fe-binding ligand
321 parameters, respectively. All results were confirmed to fall within the analytical window of the method by
322 comparing the side reaction coefficient of the added ligand α_{SA} to the side reaction coefficient of the natural

323 ligands detected (α_L). If the α_L was within an order of magnitude of α_{SA} then the results were deemed to fall
324 within the analytical window.

325 **3.3 Reverse Titration-CLE-ACSV**

326 Reverse titration-CLE-ACSV (RT-CLE-ACSV) (Hawkes et al., 2013a) was completed on 10 samples from
327 Broken Spur, and TAG hydrothermal vent fields with dFe concentrations between 19.01-90.25 nM (**Table**
328 **S31-S32**). Briefly, a 10-point titration curve was analyzed for each sample with each titration point consisting
329 of 10 mL of sample buffered with 7.5 mM boric acid and the competitive ligand 1-nitroso-2-naphthol (NN)
330 additions. All samples were analyzed on a BASi Controlled Growth Mercury Electrode (CGME) with the
331 *Epsilon Eclipse Electrochemical Analyzer* (v.213) and deposition time of 120 seconds. For each sample,
332 competitive ligand NN additions were 0.5, 1, 2, 3, 4, 6, 9, 15, 20, and 40 μ M. Samples were equilibrated
333 overnight and purged with N₂ (99.99%) for 5 minutes before analysis. At the end of each titration, three Fe
334 additions (3-15 nM) were added to the final titration point to get the total concentration of Fe in equilibrium
335 with ligands. Data was analyzed using *ElectroChemical Data Software* (v2001-2014) to acquire peak areas
336 and a package in R using the model parameters of $\beta_{FeNN3} = 5.12 \times 10^{16}$, $\chi_{min} = 0.8$, $\chi_{max} = 0.9$, and $c_{high} =$
337 0.75 to determine the Fe-binding ligand parameters (Hawkes et al., 2013a). These parameters were chosen
338 based on the recommendations for undersaturated samples and titrations curves where ip_{max} was not reached
339 (Hawkes et al., 2013a). All other parameters within the model we kept at the default values.

340 **3.4 Siderophore quantification and characterization**

341 In addition to measuring Fe-binding ligands by voltammetry, we also identified and quantified siderophores.
342 Between 0.65-1.5 L of 0.2 μ m filtered seawater pooled from ligand samples at each site (described above)
343 was pumped slowly (15-20 mL min⁻¹) onto a polystyrene-divinylbenzene (Bond Elut ENV) solid phase
344 extraction (SPE) column (Bundy et al., 2018; Boiteau et al., 2016). SPE columns were rinsed with MilliQ
345 and stored at -20°C until analysis. For the analytical measurements, samples were thawed in the dark, eluted
346 in 12 mL of distilled methanol, and dried down to between 0.2-0.5 mL of sample eluent (**Table S1**). Aliquots
347 were analyzed by reverse-phase liquid chromatography (LC) on a trace metal clean bio-inert LC (Thermo
348 Dionex 3000 NCS). The LC was interfaced with an electrospray ionization-mass spectrometer (ESI-MS;
349 Thermo Q-Exactive HF) to identify and quantify the compounds based on accurate mass (MS¹) and the
350 fragmentation (MS²) data (Bundy et al., 2018; Boiteau et al., 2016). MSconvert (Proteowizard) was used to
351 convert MS data to an open source mzXML format, and two stages of data processing were conducted using
352 modified versions of previously reported R scripts (Bundy et al., 2018; Boiteau et al., 2016). In the first stage,
353 mzXML files were read into R using new package “RaMS” (Kumler and Ingalls, 2022) , and extracted ion
354 chromatograms (EICs) were generated for each targeted m/z of interest from an in-house database of
355 siderophores. The m/z targets were the ionized apo, ⁵⁴Fe-bound, and ⁵⁶Fe-bound version of each siderophore,
356 with a tolerance of 7.5 ppm. Putative siderophore candidates were filtered through a series of hard thresholds,
357 such that MS¹ spectra were quality controlled to contain a minimum of 25 datapoints and the maximum

358 intensity of each EIC was greater than 1e4 counts. Spectra meeting these criteria and containing either ⁵⁴Fe-
359 bound and ⁵⁶Fe-bound *m/z* peaks within 30 seconds of each other or an apo peak were displayed for the user
360 to further inspect peak quality and make the final decision of whether to move on to stage two of processing
361 with a given siderophore candidate.

362

363 Stage two of processing extracted MS² spectra of the apo and Fe-bound forms of candidate siderophores to
364 compare with the predicted MS² generated by *in silico* fragmenter MetFrag (Ruttkies et al., 2016). The *in*
365 *silico* fragmenter feature was run with a tolerance of 10 ppm on “[M+H]⁺” and “[M+Na]⁺” modes. A
366 confidence level of 1-4, from highest to lowest confidence, was then assigned to putative siderophores based
367 on the following criteria: (1) peaks were present in MS¹ and MS² spectra, and at least one of the three most-
368 intense MS² fragments matched *in silico* fragmentation, (2) peaks were present in MS¹ and MS² spectra, and
369 smaller-intensity fragments matched *in silico* fragmentation, (3) peaks were present in MS¹ and MS² spectra,
370 but little to no fragments matched *in silico* fragmentation, and (4) nicely shaped peaks were identified in MS¹
371 spectra but no MS² spectra was collected (outlined in **Table S45**; example spectra in **Fig. S6-S9**). The
372 confidence levels were modelled after reporting standards for metabolite identification (Sumner et al., 2007).
373 MetFrag pulls chemical structures from publicly-available databases like PubChem or COCONUT (Sorokina
374 et al., 2021), which contain most, but not all variations of siderophores. As such, Fe-bound candidates were
375 usually run against the apo form available in the database, and for siderophores with similar structures but
376 variations in fatty chain length or double bond placement, sometimes only one parent structure was available.

377

378 A 5-point standard curve with known concentrations of siderophore ferrioxamine E was used for
379 quantification of putative siderophores, with a limit of detection of 0.257 nM in the eluent (**Fig. S10**), or
380 0.07-0.21 pM in the sample depending on sample-to-eluent volume ratio at each site (**Table S1**). MS¹ peaks
381 were integrated for all putatively identified siderophores and peak areas were converted to concentration
382 using the standard curve and the concentration factor of sample volume to eluent volume (**Fig. S10**).
383 Commercial standards are not available for most siderophores, and different compounds have distinct
384 ionization efficiencies in ESI-MS. Thus, the siderophore concentrations reported here are estimates of
385 siderophore concentrations in these environments based on ferrioxamine E, chosen for its commercial
386 availability and use in prior studies (e.g., (Boiteau et al., 2016)). Additionally, 1 mM of cyanocobalamin was
387 added as an internal standard to each sample aliquot to address any changes in sensitivity during LC-ESI-MS
388 runs. All putative siderophores that were identified with peak areas less than the detection limit were
389 discarded, and all remaining putative compounds with at least confidence levels 1 and 2 at one site were
390 included in the manuscript and are referred to as siderophores throughout. Siderophore identifications remain
391 putative due to inherent uncertainty with assignments by mass, but the confidence levels were designed such
392 that high confidence candidates contain siderophore-like moieties in their fragments. Limited sample
393 volumes prevented analysis via LC-ICP-MS like previous studies, which, in addition to greater availability
394 of commercial standards and more analytical comparisons between ferrioxamine E with other siderophore

395 types, would allow definitive characterization in future studies. Confidence level 3 and 4 putative
396 siderophores are only included in the Supplementary Information (**Table S56**). In a final step of quality
397 control, EICs for ¹³C isotopologues of candidates were inspected to verify matching peak structure.

398 **3.5 Microbial community analysis**

399 Microbial community composition was assessed in neutrally buoyant plumes and near venting sites at three
400 sites: Lucky Strike (Station 7; 1670 m), 10 km S of Rainbow (Station 17; 2000 m), and 200 km E of Rainbow
401 (Station 11; 600 m, 1600 m and 2250 m). A range of 1- 2 L of seawater were filtered by pressure filtration
402 through sequential 25 mm membrane filters housed in polypropylene filter holders (Whatman SwinLok, GE
403 Healthcare, Pittsburgh, Pennsylvania) using a peristaltic pump and silicone tubing. Samples first passed
404 through a 3 µm pore-size polyester membrane filter (Sterlitech, Auburn, Washington) then onto a 0.2 µm
405 pore-size polyethersulfone membrane filter (Supor-200, Pall Corporation, Port Washington, New York).
406 Pump tubing was acid washed with 10% hydrochloric acid and flushed with ultrapure water between each
407 sample. The filters were flash frozen in liquid nitrogen in 2 mL gasketed bead beating tubes (Fisher Scientific)
408 at sea.

409
410 Nucleic acids (DNA) were extracted as described previously (Santoro et al., 2010), with slight modifications.
411 Briefly, cells on the filters were lysed directly in the bead beating tubes with sucrose-ethylene diamine
412 tetraacetic acid (EDTA) lysis buffer (0.75 M sucrose, 20 mM EDTA, 400 mM NaCl, 50 mM Tris) and 1%
413 sodium dodecyl sulfate. Tubes were then agitated in a bead beating machine (Biospec Products) for 1 min,
414 and subsequently heated for 2 min. at 99°C in a heat block. Proteinase K (New England Biolabs) was added
415 to a final concentration of 0.5 mg/mL. Filters were incubated at 55°C for approximately 4 h and the resulting
416 lysates were purified with the DNeasy kit (Qiagen) using a slightly modified protocol (Santoro et al., 2010).
417 The purified nucleic acids were eluted in 200 µL of DNase, RNase-free water, and quantified using a
418 fluorometer (Qubit and Quanti-T HS reagent, Invitrogen Molecular Probes).

419
420 The 16S rRNA gene was amplified in all samples using V4 primers (Apprill et al., 2015; Parada et al., 2016)
421 (515F-Y and 806RB) following a previously established protocol (Stephens et al., 2020). Amplicons were
422 sequenced using a paired-end 250bp run on an Illumina MiSeq 500 and demultiplexed by the UC Davis
423 Genome Center. The resulting 16S rRNA amplicon sequences were filtered and trimmed using the DADA2
424 pipeline in R (Callahan et al., 2016). Taxonomic assignments were made with version 138.1 of the SILVA
425 SSU database (Quast et al., 2013) (silva_nr99_v138.1_wSpecies_train_set.fa.gz ;
426 doi:10.5281/zenodo.4587955; accessed March 2022). Chloroplast and mitochondrial sequences were filtered
427 out of the dataset using the 'phyloseq' R package (v 1.38.0), after which samples had read depths ranging
428 from 9375 – 65486 reads (average 28425 ± 20014 reads) and represented 1010 unique amplicon sequence
429 variants (ASVs). Read counts were transformed from absolute to relative abundance and taxa were

430 aggregated to the Family level. The ten most abundant families present in each sample were visualized using
431 the 'ggplot2' package (v. 3.3.5).

432

433 In order to assess the potential of the observed prokaryotic taxa to produce siderophores, we downloaded all
434 siderophore biosynthetic gene clusters (BGCs) in the antimash secondary metabolite database ($n = 7909$)
435 and used text-string matching to compare genera containing these BGCs to the genera found in our 16S rRNA
436 gene dataset (Blin et al., 2021). We cross-referenced the nomenclature of antimash-predicted siderophores
437 with that of the siderophores identified by LC-ESI-MS in this study, accounting for minor differences in
438 naming convention between the two databases, to determine if microbial community members present at
439 each site were predicted to make any of the siderophores that were measured at that site. Station 38 and
440 Station 12 were the closest sites with siderophore measurements for comparison against the taxonomic
441 samples taken at 200 km E of Rainbow and 10 km S of Rainbow, respectively. Samples for microbial
442 taxonomy and siderophore identity were taken from the same location at Lucky Strike and thus directly
443 compared.

444

445 **Data Availability**

446 The CSV data reported in this study has been deposited at Zenodo under the DOI:
447 <http://doi.org/10.5281/zenodo.7325154>. The LC-ES-MS data has been deposited on Massive under the DOI:
448 <http://doi.org/doi.10.25345/C5V97ZW7N>. Microbial 16S rRNA data have been deposited on GenBank under
449 the accession number BioProject #PRJNA865382. All data is freely available on each of these data
450 repositories.

451

452

453 **Acknowledgments**

454 We acknowledge the captain and crew of the R/V *James Cook*, Chief Scientist Alessandro Tagliabue, and
455 Noah Gluschankoff for supporting this work. This study was a part of the FeRidge project (GEOTRACES
456 section GA13) which was supported by the Natural Environment Research Council funding (NERC United
457 Kingdom Grants NE/N010396/1 to MCL and NE/N009525/1 to AT). The International GEOTRACES
458 Programme is possible in part thanks to the support from the U.S. National Science Foundation (Grant OCE-
459 1840868) to the Scientific Committee on Oceanic Research (SCOR). CLH was funded by JISAO/CICOES
460 postdoctoral fellowship. PJM was funded through the NOAA Hollings Scholar summer program. JR was
461 funded by NOAA Ocean Exploration and Research, NOAA Earth-Ocean Interactions programs at NOAA-
462 Pacific Marine Environmental Lab (PMEL #5955), and UW-CICOES (CICOES #2024-1385). ~~JR was funded~~
463 ~~by NOAA Ocean Exploration and Research, NOAA Earth-Ocean Interactions programs at NOAA Pacific~~
464 ~~Marine Environmental Labs, and JISAO/CICOES.~~ Part of this work was carried out in the University of
465 Washington TraceLab, which receives support from the M.J. Murdock Charitable Trust in conjunction with
466 the University of Washington College of Environment, and the Pacific Marine Environmental Labs at the

467 National Oceanic and Atmospheric Administration. Parts of this work was also carried out in Dr. Anitra
468 Ingalls laboratory with the help of Laura Truxal and Dr. Jiwoon Park at the University of Washington-School
469 of Oceanography.

470

471 **Author Contributions:** Manuscript preparation, sample/data processing, CSV analysis, and interpretation
472 LC-ESI-MS data analysis and interpretation (C.L.H. and P.J.M.), microbial analysis and interpretation
473 (J.B.A. and A.E.S.), dissolved iron and derived excess $^3\text{He}_{\text{xs}}$ measurements, sample collection (A.J.M. L. and
474 M.C.L.), microbial data collection and ligand data interpretation (T.M. and K.N.B.), and project design and
475 planning, data interpretation, and mentoring (A.T., M.C.L., J.A.R., and R.M.B.). All authors were involved
476 in editing and revision of the manuscript.

477

478 **Competing Interest Statement:** The authors declare no competing interests.

479

480 **References**

481 Abualhaija, M. M. and van den Berg, C. M. G. G.: Chemical speciation of iron in seawater using catalytic
482 cathodic stripping voltammetry with ligand competition against salicylaldehyde, *Mar. Chem.*, 164, 60–74,
483 <https://doi.org/10.1016/j.marchem.2014.06.005>, 2014.

484 Aguilar-Islas, A. M., Wu, J., Rember, R., Johansen, A. M., and Shank, L. M.: Dissolution of aerosol-derived
485 iron in seawater: Leach solution chemistry, aerosol type, and colloidal iron fraction, *Mar. Chem.*, 120, 25–
486 33, 2010.

487 Apprill, A., McNally, S., Parsons, R., and Weber, L.: Minor revision to V4 region SSU rRNA 806R gene
488 primer greatly increases detection of SAR11 bacterioplankton, *Aquat. Microb. Ecol.*, 75, 129–137,
489 <https://doi.org/10.3354/ame01753>, 2015.

490 Bazylev, B. A.: Allochemical Metamorphism of Mantle Peridotites in the Hayes Fracture Zone of the North
491 Atlantic, *Petrology*, 5, 362–379, 1997.

492 Beaulieu, S. E. and Szafranski, K. M.: InterRidge Global Database of Active Submarine Hydrothermal Vent
493 Fields Version 3.4, <https://doi.org/10.1594/PANGAEA.917894>, 2020.

494 Bennett, S. a., Achterberg, E. P., Connelly, D. P., Statham, P. J., Fones, G. R., and German, C. R.: The
495 distribution and stabilisation of dissolved Fe in deep-sea hydrothermal plumes, *Earth Planet. Sci. Lett.*, 270,
496 157–167, <https://doi.org/10.1016/j.epsl.2008.01.048>, 2008.

497 Bennett, S. a., Hansman, R. L., Sessions, A. L., Nakamura, K. ichi, and Edwards, K. J.: Tracing iron-fueled
498 microbial carbon production within the hydrothermal plume at the Loihi seamount, *Geochim. Cosmochim.*
499 *Acta*, 75, 5526–5539, <https://doi.org/10.1016/j.gca.2011.06.039>, 2011.

500 Blin, K., Shaw, S., Kautsar, S. A., Medema, M. H., and Weber, T.: The antiSMASH database version 3:
501 Increased taxonomic coverage and new query features for modular enzymes, *Nucleic Acids Res.*, 49, D639–
502 D643, <https://doi.org/10.1093/nar/gkaa978>, 2021.

503 Boiteau, R. M., Mende, D. R., Hawco, N. J., McIlvin, M. R., Fitzsimmons, J. N., Saito, M. A., Sedwick, P.
504 N., DeLong, E. F., and Repeta, D. J.: Siderophore-based microbial adaptations to iron scarcity across the
505 eastern Pacific Ocean, *Proc. Natl. Acad. Sci.*, 113, 14237–14242, <https://doi.org/10.1073/pnas.1608594113>,

506 2016.

507 Boiteau, R. M., Till, C. P., Coale, T. H., Fitzsimmons, J. N., Bruland, K. W., and Repeta, D. J.: Patterns of
508 iron and siderophore distributions across the California Current System, *Limnol. Oceanogr.*, 64, 376–389,
509 <https://doi.org/10.1002/lno.11046>, 2019.

510 Buck, K. N., Sohst, B., and Sedwick, P. N.: The organic complexation of dissolved iron along the U.S.
511 GEOTRACES (GA03) North Atlantic Section, *Deep. Res. Part II Top. Stud. Oceanogr.*, 116, 152–165,
512 <https://doi.org/10.1016/j.dsr2.2014.11.016>, 2015.

513 Buck, K. N., Sedwick, P. N., Sohst, B., and Carlson, C. A.: Organic complexation of iron in the eastern
514 tropical South Pacific: Results from US GEOTRACES Eastern Pacific Zonal Transect (GEOTRACES cruise
515 GP16), *Mar. Chem.*, 201, 229–241, <https://doi.org/10.1016/j.marchem.2017.11.007>, 2018.

516 Bundy, R. M., Boiteau, R. M., McLean, C., Turk-Kubo, K. A., McIlvin, M. R., Saito, M. A., Mooy, B. A.
517 Van, and Repeta, D. J.: Distinct Siderophores Contribute to Iron Cycling in the Mesopelagic at Station
518 ALOHA, *Front. Mar. Sci.*, 1–15, <https://doi.org/10.3389/fmars.2018.00061>, 2018.

519 Butler, A.: Marine siderophores and microbial iron mobilization., *Biometals*, 18, 369–374,
520 <https://doi.org/10.1007/s10534-005-3711-0>, 2005.

521 Butler, A. and Theisen, R. M.: Iron(III)-siderophore coordination chemistry: Reactivity of marine
522 siderophores., *Coord. Chem. Rev.*, 254, 288–296, <https://doi.org/10.1016/j.ccr.2009.09.010>, 2010.

523 Callahan, B. J., McMurdie, P. J., Rosen, M. J., Han, A. W., Johnson, A. J. A., and Holmes, S. P.: DADA2:
524 High-resolution sample inference from Illumina amplicon data, *Nat. Methods*, 13, 581–583,
525 <https://doi.org/10.1038/nmeth.3869>, 2016.

526 Carmichael, J. R., Zhou, H., and Butler, A.: A suite of asymmetric citrate siderophores isolated from a marine
527 *Shewanella* species, *J. Inorg. Biochem.*, 198, 1–6, <https://doi.org/10.1016/j.jinorgbio.2019.110736>, 2019.

528 Cowen, J. P. and Bruland, K. W.: Metal deposits associated with bacteria: implications for Fe and Mn marine
529 biogeochemistry, *Deep Sea Res. Part A. Oceanogr. Res. Pap.*, 32, 253–272, [https://doi.org/10.1016/0198-0149\(85\)90078-0](https://doi.org/10.1016/0198-0149(85)90078-0), 1985.

531 Cowen, J. P., Massoth, G. J., and Feely, R. A.: Scavenging rates of dissolved manganese in a hydrothermal
532 vent plume, *Deep Sea Res. Part A. Oceanogr. Res. Pap.*, 37, 1619–1637, [https://doi.org/10.1016/0198-0149\(90\)90065-4](https://doi.org/10.1016/0198-0149(90)90065-4), 1990.

534 Crowley, D. E., Wang, Y. C., Reid, C. P. P., and Szanislo, P. J.: Mechanisms of iron acquisition from
535 siderophores by microorganisms and plants, *Plant Soil*, 130, 179–198, 1991.

536 Dick, G. J., Anantharaman, K., Baker, B. J., Li, M., Reed, D. C., and Sheik, C. S.: The microbiology of deep-
537 sea hydrothermal vent plumes: ecological and biogeographic linkages to seafloor and water column habitats.,
538 *Front. Microbiol.*, 4, 124, <https://doi.org/10.3389/fmicb.2013.00124>, 2013.

539 Fishwick, M. P., Sedwick, P. N., Lohan, M. C., Worsfold, P. J., Buck, K. N., Church, T. M., and Ussher, S.
540 J.: The impact of changing surface ocean conditions on the dissolution of aerosol iron, *Global Biogeochem.*
541 *Cycles*, 28, 1235–1250, <https://doi.org/10.1002/2014GB004921>, 2014.

542 Fitzsimmons, J. N., Boyle, E. a., and Jenkins, W. J.: Distal transport of dissolved hydrothermal iron in the
543 deep South Pacific Ocean, *Proc. Natl. Acad. Sci.*, 111, 16654–16661,
544 <https://doi.org/10.1073/pnas.1418778111>, 2014.

545 Fitzsimmons, J. N., John, S. G., Marsay, C. M., Hoffman, C. L., Nicholas, S. L., Toner, B. M., German, C.
546 R., and Sherrell, R. M.: Iron persistence in the distal hydrothermal plume supported by dissolved – particulate
547 exchange, *Nat. Geosci.*, 10, 1–8, <https://doi.org/10.1038/ngeo2900>, 2017.

- 548 German, C. and Seyfried, W. E.: Hydrothermal Processes, 2nd ed., Elsevier Ltd., 1–39 pp.,
549 <https://doi.org/10.1016/B978-0-08-095975-7.00201-1>, 2014.
- 550 Gledhill, M. and Buck, K. N.: The organic complexation of iron in the marine environment: A review, *Front.*
551 *Microbiol.*, 3, 1–17, <https://doi.org/10.3389/fmicb.2012.00069>, 2012.
- 552 Gu, H., Sun, Q., Luo, J., Zhang, J., and Sun, L.: A First Study of the Virulence Potential of a *Bacillus subtilis*
553 Isolate From Deep-Sea Hydrothermal Vent, *Front. Cell. Infect. Microbiol.*, 9, 1–14,
554 <https://doi.org/10.3389/fcimb.2019.00183>, 2019.
- 555 Hassler, C. S., van den Berg, C. M. G., and Boyd, P. W.: Toward a regional classification to provide a more
556 inclusive examination of the ocean biogeochemistry of iron-binding ligands, *Front. Mar. Sci.*, 4,
557 <https://doi.org/10.3389/fmars.2017.00019>, 2017.
- 558 Hawkes, J. A., Gledhill, M., Connelly, D. P., and Achterberg, E. P.: Characterisation of iron binding ligands
559 in seawater by reverse titration, *Anal. Chim. Acta*, 766, 53–60, <https://doi.org/10.1016/j.aca.2012.12.048>,
560 2013a.
- 561 Hawkes, J. A., Connelly, D. P., Gledhill, M., and Achterberg, E. P.: The stabilisation and transportation of
562 dissolved iron from high temperature hydrothermal vent systems, *Earth Planet. Sci. Lett.*, 375, 280–290,
563 <https://doi.org/10.1016/j.epsl.2013.05.047>, 2013b.
- 564 Hawkes, J. A., Connelly, D. P., Gledhill, M., and Achterberg, E. P.: The stabilisation and transportation of
565 dissolved iron from high temperature hydrothermal vent systems, *Earth Planet. Sci. Lett.*, 375, 280–290,
566 <https://doi.org/10.1016/j.epsl.2013.05.047>, 2013c.
- 567 Hider, R. C. and Kong, X.: Chemistry and biology of siderophores, *Nat. Prod. Rep.*, 27, 637–657,
568 <https://doi.org/10.1039/b906679a>, 2010.
- 569 Hoffman, C. L., Nicholas, S. L., Ohnemus, D. C., Fitzsimmons, J. N., Sherrell, R. M., German, C. R., Heller,
570 M. I., Lee, J. mi, Lam, P. J., and Toner, B. M.: Near-field iron and carbon chemistry of non-buoyant
571 hydrothermal plume particles, Southern East Pacific Rise 15°S, *Mar. Chem.*, 201, 183–197,
572 <https://doi.org/10.1016/j.marchem.2018.01.011>, 2018.
- 573 Hoffman, C. L., Schladweiler, C., Seaton, N. C. A., Nicholas, S. L., Fitzsimmons, J., Sherrell, R. M., German,
574 C. R., Lam, P., and Toner, B. M.: Diagnostic morphology and solid-state chemical speciation of
575 hydrothermally derived particulate Fe in a long-range dispersing plume, *ACS Earth Sp. Chem.*, 4, 1831–
576 1842, <https://doi.org/10.1021/acsearthspacechem.0c00067>, 2020.
- 577 Holden, J., Breier, J., Rogers, K., Schulte, M., and Toner, B.: Biogeochemical processes at hydrothermal
578 vents: microbes and minerals, bioenergetics, and carbon fluxes, *Oceanography*, 25, 196–208,
579 <https://doi.org/http://dx.doi.org/10.5670/oceanog.2012.18>, 2012.
- 580 Homann, V. V., Sandy, M., Tincu, J. A., Templeton, A. S., Tebo, B. M., and Butler, A.: Loihichelins A - F ,
581 a Suite of Amphiphilic Siderophores Produced by the Marine Bacterium *Halomonas LOB-5*, *J. Nat. Prod.*,
582 72, 884–888, 2009.
- 583 Honeyman, B. D. and Santschi, P. H.: A Brownian-pumping model for oceanic trace metal scavenging:
584 evidence from Th isotopes, 1989.
- 585 Kato, C. and Nogi, Y.: Correlation between phylogenetic structure and function : examples from deep-sea
586 *Shewanella*, 35, 223–230, 2001.
- 587 Kelley, D. S. and Shank, T. M.: Hydrothermal systems: A decade of discovery in slow spreading
588 environments, *Geophys. Monogr. Ser.*, 188, 369–407, <https://doi.org/10.1029/2010GM000945>, 2010.
- 589 Kleint, C., Hawkes, J. A., Sander, S. G., and Koschinsky, A.: Voltammetric Investigation of Hydrothermal
590 Iron Speciation, *Front. Mar. Sci.*, 3, 1–11, <https://doi.org/10.3389/fmars.2016.00075>, 2016.

591 Kuhn, K. M., Maurice, P. A., States, U., Neubauer, E., Hofmann, T., and Kammer, F. Von Der: Accessibility
592 of Humic-Associated Fe to a Microbial Siderophore: Implications for Bioavailability, *Environ. Sci. Technol.*,
593 1015–1022, 2014.

594 Kumler, W. and Ingalls, A. E.: The R Journal: Tidy Data Neatly Resolves Mass-Spectrometry’s Ragged
595 Arrays, *R J.*, 2022.

596 Laglera, L. M. and van den Berg, C. M. G.: Evidence for geochemical control of iron by humic substances
597 in seawater, *Limnol. Oceanogr.*, 54, 610–619, 2009.

598 Lauderdale, J. M., Braakman, R., Forget, G., Dutkiewicz, S., and Follows, M. J.: Microbial feedbacks
599 optimize ocean iron availability, *Proc. Natl. Acad. Sci. U. S. A.*, 117, 4842–4849,
600 <https://doi.org/10.1073/pnas.1917277117>, 2020.

601 Li, M., Toner, B. M., Baker, B. J., Breier, J. a, Sheik, C. S., and Dick, G. J.: Microbial iron uptake as a
602 mechanism for dispersing iron from deep-sea hydrothermal vents., *Nat. Commun.*, 5, 3192,
603 <https://doi.org/10.1038/ncomms4192>, 2014.

604 Lough, A. J. M., Tagliabue, A., Demasy, C., Resing, J. A., Mellett, T., Wyatt, N. J., and Lohan, M. C.: The
605 impact of hydrothermal vent geochemistry on the addition of iron to the deep ocean, *Biogeosciences Discuss.*,
606 [preprint], 1–23, <https://doi.org/10.5194/bg-2022-73>, 2022.

607 Mackey, D. J. and Zirino, A.: Comments on trace metal speciation in seawater or do “onions” grow in the
608 sea?, *Anal. Chim. Acta*, 284, 635–647, 1994.

609 Manck, L. E., Park, J., Tully, B. J., Poire, A. M., Bundy, R. M., Dupont, C. L., and Barbeau, K. A.:
610 Petrobactin, a siderophore produced by *Alteromonas*, mediates community iron acquisition in the global
611 ocean, *ISME J.*, 16, 358–369, <https://doi.org/10.1038/s41396-021-01065-y>, 2022.

612 Martinez, J. S., Carter-Franklin, J. N., Mann, E. L., Martin, J. D., Haygood, M. G., and Butler, A.: Structure
613 and membrane affinity of a suite of amphiphilic siderophores produced by a marine bacterium, *Proc. Natl.*
614 *Acad. Sci. U. S. A.*, 100, 3754–3759, <https://doi.org/10.1073/pnas.0637444100>, 2003.

615 Mellett, T., Albers, J. B., Santoro, A., Wang, W., Salaun, P., Resing, J., Lough, A. J. ., Tagliabue, A., Lohan,
616 M., Bundy, R. M., and Buck, K. N.: Particle exchange mediated by organic ligands in incubation experiments
617 of hydrothermal vent plumes along the mid-Atlantic Ridge, n.d.

618 Misumi, K., Lindsay, K., Moore, J. K., Doney, S. C., Tsumune, D., and Yoshida, Y.: Humic substances may
619 control dissolved iron distributions in the global ocean: Implications from numerical simulations, *Global*
620 *Biogeochem. Cycles*, 27, 450–462, 2013.

621 Moore, L. E., Heller, M. I., Barbeau, K. A., Moffett, J. W., and Bundy, R. M.: Organic complexation of iron
622 by strong ligands and siderophores in the eastern tropical North Pacific oxygen deficient zone, *Mar. Chem.*,
623 236, 104021, <https://doi.org/10.1016/j.marchem.2021.104021>, 2021.

624 Muller, F. L. L.: Exploring the Potential Role of Terrestrially Derived Humic Substances in the Marine
625 Biogeochemistry of Iron, *Front. Earth Sci.*, 6, 1–20, <https://doi.org/10.3389/feart.2018.00159>, 2018.

626 Omanović, D., Garnier, C., and Pižeta, I.: ProMCC: An all-in-one tool for trace metal complexation studies,
627 *Mar. Chem.*, 173, 25–39, <https://doi.org/10.1016/j.marchem.2014.10.011>, 2015.

628 Parada, A. E., Needham, D. M., and Fuhrman, J. A.: Every base matters: Assessing small subunit rRNA
629 primers for marine microbiomes with mock communities, time series and global field samples, *Environ.*
630 *Microbiol.*, 18, 1403–1414, <https://doi.org/10.1111/1462-2920.13023>, 2016.

631 Park, J., Durham, B. P., Key, R. S., Groussman, R. D., Pinedo-Gonzalez, P., Hawco, N. J., John, S. G.,
632 Carlson, M. C. G., Lindell, D., Juranek, L., Ferrón, S., Ribalet, F., Armbrust, E. V., Ingalls, A. E., and Bundy,
633 R. M.: Siderophore production and utilization by microbes in the North Pacific Ocean, *bioRxiv*,

634 2022.02.26.482025, <https://doi.org/10.1101/2022.02.26.482025>, 2022.

635 Park, J., Durham, B. P., Key, R. S., Groussman, R. D., Bartolek, Z., Pinedo-Gonzalez, P., Hawco, N. J., John,
636 S. G., Carlson, M. C. G., and Lindell, D.: Siderophore production and utilization by marine bacteria in the
637 North Pacific Ocean, *Limnol. Oceanogr.*, 68, 1636–1653, 2023a.

638 Park, J., Durham, B. P., Key, R. S., Groussman, R. D., Pinedo-Gonzalez, P., Hawco, N. J., John, S. G.,
639 Carlson, M. C. G., Lindell, D., Juranek, L., Ferrón, S., Ribalet, F., Armbrust, E. V., Ingalls, A. E., and Bundy,
640 R. M.: Siderophore production and utilization by microbes in the North Pacific Ocean, *Limnol. Oceanogr.*,
641 2022.02.26.482025, <https://doi.org/10.1002/lno.12373>, 2023b.

642 Quast, C., Pruesse, E., Yilmaz, P., Gerken, J., Schweer, T., Yarza, P., Peplies, J., and Glöckner, F. O.: The
643 SILVA ribosomal RNA gene database project: Improved data processing and web-based tools, *Nucleic Acids*
644 *Res.*, 41, 590–596, <https://doi.org/10.1093/nar/gks1219>, 2013.

645 Reitz, Z. L., Butler, A., and Medema, M. H.: Automated genome mining predicts combinatorial diversity and
646 taxonomic distribution of peptide metallophore structures, *bioRxiv*, 15–20,
647 <https://doi.org/https://doi.org/10.1101/2022.12.14.519525>, 2022.

648 Resing, J. a., Sedwick, P. N., German, C. R., Jenkins, W. J., Moffett, J. W., Sohst, B. M., and Tagliabue, A.:
649 Basin-scale transport of hydrothermal dissolved metals across the South Pacific Ocean, *Nature*, 523, 200–
650 203, <https://doi.org/10.1038/nature14577>, 2015.

651 Rizzi, A., Roy, S., Bellenger, J. P., and Beaugerard, P. B.: Iron homeostasis in *Bacillus subtilis* requires
652 siderophore production and biofilm formation, *Appl. Environ. Microbiol.*, 85,
653 <https://doi.org/10.1128/AEM.02439-18>, 2019.

654 Ruttkies, C., Schymanski, E. L., Wolf, S., Hollender, J., and Neumann, S.: MetFrag relaunched: incorporating
655 strategies beyond in silico fragmentation, *J. Cheminform.*, 8, 1–16, <https://doi.org/10.1186/s13321-016-0115-9>, 2016.

657 Sander, S. G. and Koschinsky, A.: Metal flux from hydrothermal vents increased by organic complexation,
658 *Nat. Geosci.*, 4, 145–150, <https://doi.org/10.1038/ngeo1088>, 2011.

659 Sandy, M. and Butler, A.: Microbial iron acquisition: marine and terrestrial siderophores., *Chem. Rev.*, 109,
660 4580–95, <https://doi.org/10.1021/cr9002787>, 2009.

661 Santoro, A. E., Casciotti, K. L., and Francis, C. A.: Activity, abundance and diversity of nitrifying archaea
662 and bacteria in the central California Current, *Environ. Microbiol.*, 12, 1989–2006,
663 <https://doi.org/10.1111/j.1462-2920.2010.02205.x>, 2010.

664 Sheik, C. S., Anantharaman, K., Breier, J. A., Sylvan, J. B., Edwards, K. J., and Dick, G. J.: Spatially resolved
665 sampling reveals dynamic microbial communities in rising hydrothermal plumes across a back-arc basin.,
666 *ISME J.*, 9, 1434–45, <https://doi.org/10.1038/ismej.2014.228>, 2015.

667 Sorokina, M., Merseburger, P., Rajan, K., Yirik, M. A., and Steinbeck, C.: COCONUT online: Collection of
668 Open Natural Products database, *J. Cheminform.*, 13, 1–13, <https://doi.org/10.1186/s13321-020-00478-9>,
669 2021.

670 Stephens, B. M., Opalk, K., Petras, D., Liu, S., Comstock, J., Aluwihare, L. I., Hansell, D. A., and Carlson,
671 C. A.: Organic Matter Composition at Ocean Station Papa Affects Its Bioavailability, *Bacterioplankton*
672 *Growth Efficiency and the Responding Taxa*, *Front. Mar. Sci.*, 7, <https://doi.org/10.3389/fmars.2020.590273>,
673 2020.

674 Sumner, L. W., Amberg, A., Barrett, D., Beale, M. H., Beger, R., Daykin, C. A., Fan, T. W.-M., Fiehn, O.,
675 Goodacre, R., Griffin, J. L., Hankemeier, T., Hardy, N., Harnly, J., Higashi, R., Kopka, J., Lane, A. N.,
676 Lindon, J. C., Marriott, P., Nicholls, A. W., Reily, M. D., Thaden, J. J., and Viant, M. R.: Proposed minimum
677 reporting standards for chemical analysis, *Metabolomics*, 3, 211–221,

678 0082-2, 2007.

679 Tagliabue, A., Bowie, A. R., Boyd, P. W., Buck, K. N., Johnson, K. S., and Saito, M. A.: The integral role
680 of iron in ocean biogeochemistry, *Nature*, 543, 51–59, <https://doi.org/10.1038/nature21058>, 2017.

681 Toner, B. M., Fakra, S. C., Manganini, S. J., Santelli, C. M., Marcus, M. a., Moffett, J. W., Rouxel, O.,
682 German, C. R., and Edwards, K. J.: Preservation of iron(II) by carbon-rich matrices in a hydrothermal plume,
683 *Nat. Geosci.*, 2, 197–201, <https://doi.org/10.1038/ngeo433>, 2009.

684 Tortell, P. D., Maldonado, M. T., and Price, N. M.: The role of heterotrophic bacteria in iron-limited ocean
685 ecosystems, *Nature*, 383, 330–332, <https://doi.org/10.1038/383330a0>, 1996.

686 Vraspir, J. M. and Butler, A.: Chemistry of marine ligands and siderophores., *Ann. Rev. Mar. Sci.*, 1, 43–63,
687 <https://doi.org/10.1146/annurev.marine.010908.163712>, 2009.

688 Wang, H., Wang, W., Liu, M., Zhou, H., Ellwood, M. J., Butterfield, D. A., Buck, N. J., and Resing, J. A.:
689 Iron ligands and isotopes in hydrothermal plumes over backarc volcanoes in the Northeast Lau Basin,
690 Southwest Pacific Ocean, *Geochim. Cosmochim. Acta*, 336, 341–352, 2022.

691 Waska, H., Koschinsky, A., Ruiz Chanco, M. J., and Dittmar, T.: Investigating the potential of solid-phase
692 extraction and Fourier-transform ion cyclotron resonance mass spectrometry (FT-ICR-MS) for the isolation
693 and identification of dissolved metal-organic complexes from natural waters, *Mar. Chem.*, 173, 78–92,
694 <https://doi.org/10.1016/j.marchem.2014.10.001>, 2015.

695 Whitby, H., Planquette, H., Cassar, N., Bucciarelli, E., Osburn, C. L., Janssen, D. J., Cullen, J. T., González,
696 A. G., Völker, C., and Sarthou, G.: A call for refining the role of humic-like substances in the oceanic iron
697 cycle, *Sci. Rep.*, 10, 6144, 2020.

698 Whitby, H., Park, J., Shaked, Y., Boiteau, R. M., Buck, K. N., and Bundy, R. M.: New insights into the
699 organic complexation of bioactive trace metals in the global ocean from the GEOTRACES era,
700 *Oceanography*, 37, 142–155, 2024.

701 Yücel, M., Gartman, A., Chan, C. S., and Luther, G. W.: Hydrothermal vents as a kinetically stable source
702 of iron-sulphide-bearing nanoparticles to the ocean, *Nat. Geosci.*, 4, 367–371,
703 <https://doi.org/10.1038/ngeo1148>, 2011.

704 ~~[Abualhaija, M. M. and van den Berg, C. M. G. G.: Chemical speciation of iron in seawater using catalytic](#)~~
705 ~~[cathodic stripping voltammetry with ligand competition against salicylaldoxime, *Mar. Chem.*, 164, 60–74,](#)~~
706 ~~<https://doi.org/10.1016/j.marchem.2014.06.005>, 2014.~~

707 ~~[Apprill, A., Menally, S., Parsons, R., and Weber, L.: Minor revision to V4 region SSU rRNA 806R gene](#)~~
708 ~~[primer greatly increases detection of SAR11 bacterioplankton, *Aquat. Microb. Ecol.*, 75, 129–137,](#)~~
709 ~~<https://doi.org/10.3354/ame01753>, 2015.~~

710 ~~[Bazylev, B. A.: Allochemical Metamorphism of Mantle Peridotites in the Hayes Fracture Zone of the North](#)~~
711 ~~[Atlantic, *Petrology*, 5, 362–379, 1997.](#)~~

712 ~~[Beaulieu, S. E. and Szafranski, K. M.: InterRidge Global Database of Active Submarine Hydrothermal Vent](#)~~
713 ~~[Fields Version 3.4, <https://doi.org/10.1594/PANGAEA.917894>, 2020.](#)~~

714 ~~[Bennett, S. a., Achterberg, E. P., Connelly, D. P., Statham, P. J., Fones, G. R., and German, C. R.: The](#)~~
715 ~~[distribution and stabilisation of dissolved Fe in deep-sea hydrothermal plumes, *Earth Planet. Sci. Lett.*, 270,](#)~~
716 ~~[157–167, https://doi.org/10.1016/j.epsl.2008.01.048](https://doi.org/10.1016/j.epsl.2008.01.048), 2008.~~

717 ~~[Bennett, S. a., Hansman, R. L., Sessions, A. L., Nakamura, K. ichi, and Edwards, K. J.: Tracing iron-fueled](#)~~
718 ~~[microbial carbon production within the hydrothermal plume at the Loihi seamount, *Geochim. Cosmochim.*](#)~~
719 ~~[Acta](#), 75, 5526–5539, <https://doi.org/10.1016/j.gca.2011.06.039>, 2011.~~

720 [Blin, K., Shaw, S., Kautsar, S. A., Medema, M. H., and Weber, T.: The antiSMASH database version 3:
721 \[Increased taxonomic coverage and new query features for modular enzymes, *Nucleic Acids Res.*, 49, D639–
722 \\[D643, <https://doi.org/10.1093/nar/gkaa978>, 2021.\\]\\(#\\)\]\(#\)](#)

723 [Boiteau, R. M., Mende, D. R., Hawco, N. J., Mellvin, M. R., Fitzsimmons, J. N., Saito, M. A., Sedwick, P.
724 \[N., DeLong, E. F., and Repeta, D. J.: Siderophore based microbial adaptations to iron scarcity across the
725 \\[eastern Pacific Ocean, *Proc. Natl. Acad. Sci.*, 113, 14237–14242, <https://doi.org/10.1073/pnas.1608594113>,
726 \\\[2016.\\\]\\\(#\\\)\\]\\(#\\)\]\(#\)](#)

727 [Boiteau, R. M., Till, C. P., Coale, T. H., Fitzsimmons, J. N., Bruland, K. W., and Repeta, D. J.: Patterns of
728 \[iron and siderophore distributions across the California Current System, *Limnol. Oceanogr.*, 64, 376–389,
729 \\[https://doi.org/10.1002/lno.11046\\]\\(#\\), 2019.\]\(#\)](#)

730 [Buck, K. N., Lohan, M. C., Berger, C. J. M., and Bruland, K. W.: Dissolved iron speciation in two distinct
731 \[river plumes and an estuary: Implications for riverine iron supply, *Limnol. Oceanogr.*, 52, 843–855,
732 \\[https://doi.org/10.4319/lno.2007.52.2.0843\\]\\(#\\), 2007.\]\(#\)](#)

733 [Buck, K. N., Sohst, B., and Sedwick, P. N.: The organic complexation of dissolved iron along the U.S.
734 \[GEOTRACES \\(GA03\\) North Atlantic Section, *Deep. Res. Part II Top. Stud. Oceanogr.*, 116, 152–165,
735 \\[https://doi.org/10.1016/j.dsr2.2014.11.016\\]\\(#\\), 2015.\]\(#\)](#)

736 [Buck, K. N., Sedwick, P. N., Sohst, B., and Carlson, C. A.: Organic complexation of iron in the eastern
737 \[tropical South Pacific: Results from US GEOTRACES Eastern Pacific Zonal Transect \\(GEOTRACES cruise
738 \\[GP16\\\), *Mar. Chem.*, 201, 229–241, <https://doi.org/10.1016/j.marehem.2017.11.007>, 2018.\\]\\(#\\)\]\(#\)](#)

739 [Bundy, R. M., Abdulla, H. A. N., Hatcher, P. G., Biller, D. V., Buck, K. N., and Barbeau, K. A.: Iron binding
740 \[ligands and humic substances in the San Francisco Bay estuary and estuarine influenced shelf regions of
741 \\[coastal California, *Mar. Chem.*, 173, 183–194, <https://doi.org/10.1016/j.marehem.2014.11.005>, 2015.\\]\\(#\\)\]\(#\)](#)

742 [Bundy, R. M., Boiteau, R. M., McLean, C., Turk Kubo, K. A., McIlvin, M. R., Saito, M. A., Mooy, B. A.
743 \[Van, and Repeta, D. J.: Distinct Siderophores Contribute to Iron Cycling in the Mesopelagic at Station
744 \\[ALOHA, *Front. Mar. Sci.*, 1–15, <https://doi.org/10.3389/fmars.2018.00061>, 2018.\\]\\(#\\)\]\(#\)](#)

745 [Butler, A.: Marine siderophores and microbial iron mobilization., *Biometals*, 18, 369–374,
746 \[https://doi.org/10.1007/s10534-005-3711-0\]\(#\), 2005.](#)

747 [Butler, A. and Theisen, R. M.: Iron\(III\) siderophore coordination chemistry: Reactivity of marine
748 \[siderophores., *Coord. Chem. Rev.*, 254, 288–296, <https://doi.org/10.1016/j.ccr.2009.09.010>, 2010.\]\(#\)](#)

749 [Callahan, B. J., McMurdie, P. J., Rosen, M. J., Han, A. W., Johnson, A. J. A., and Holmes, S. P.: DADA2:
750 \[High resolution sample inference from Illumina amplicon data, *Nat. Methods*, 13, 581–583,
751 \\[https://doi.org/10.1038/nmeth.3869\\]\\(#\\), 2016.\]\(#\)](#)

752 [Carmichael, J. R., Zhou, H., and Butler, A.: A suite of asymmetric citrate siderophores isolated from a marine
753 \[Shewanella species, *J. Inorg. Biochem.*, 198, 1–6, <https://doi.org/10.1016/j.jinorgbio.2019.110736>, 2019.\]\(#\)](#)

754 [Cowen, J. P. and Bruland, K. W.: Metal deposits associated with bacteria: implications for Fe and Mn marine
755 \[biogeochemistry, *Deep Sea Res. Part A. Oceanogr. Res. Pap.*, 32, 253–272, \\[0149\\\(85\\\)90078-0\\]\\(https://doi.org/10.1016/0198-
756 <a href=\\), 1985.\]\(#\)](#)

757 [Cowen, J. P., Massoth, G. J., and Feely, R. A.: Seavenging rates of dissolved manganese in a hydrothermal
758 \[vent plume, *Deep Sea Res. Part A. Oceanogr. Res. Pap.*, 37, 1619–1637, \\[0149\\\(90\\\)90065-4\\]\\(https://doi.org/10.1016/0198-
759 <a href=\\), 1990.\]\(#\)](#)

760 [Crowley, D. E., Wang, Y. C., Reid, C. P. P., and Szaniszló, P. J.: Mechanisms of iron acquisition from
761 \[siderophores by microorganisms and plants, *Plant Soil*, 130, 179–198, 1991.\]\(#\)](#)

762 [Fishwick, M. P., Sedwick, P. N., Lohan, M. C., Worsfold, P. J., Buck, K. N., Church, T. M., and Ussher, S.](#)

763 J.: The impact of changing surface ocean conditions on the dissolution of aerosol iron, *Global Biogeochem.*
764 *Cycles*, 28, 1235–1250, <https://doi.org/10.1002/2014GB004921>, 2014.

765 Fitzsimmons, J. N., John, S. G., Marsay, C. M., Hoffman, C. L., Nicholas, S. L., Toner, B. M., German, C.
766 R., and Sherrell, R. M.: Iron persistence in the distal hydrothermal plume supported by dissolved–particulate
767 exchange, *Nat. Geosci.*, 10, 1–8, <https://doi.org/10.1038/ngeo2900>, 2017.

768 Gu, H., Sun, Q., Luo, J., Zhang, J., and Sun, L.: A First Study of the Virulence Potential of a *Bacillus subtilis*
769 Isolate From Deep Sea Hydrothermal Vent, *Front. Cell. Infect. Microbiol.*, 9, 1–14,
770 <https://doi.org/10.3389/fcimb.2019.00183>, 2019.

771 Hawkes, J. A., Gledhill, M., Connelly, D. P., and Achterberg, E. P.: Characterisation of iron binding ligands
772 in seawater by reverse titration, *Anal. Chim. Acta*, 766, 53–60, <https://doi.org/10.1016/j.aca.2012.12.048>,
773 2013a.

774 Hawkes, J. A., Connelly, D. P., Gledhill, M., and Achterberg, E. P.: The stabilisation and transportation of
775 dissolved iron from high temperature hydrothermal vent systems, *Earth Planet. Sci. Lett.*, 375, 280–290,
776 <https://doi.org/10.1016/j.epsl.2013.05.047>, 2013b.

777 Hider, R. C. and Kong, X.: Chemistry and biology of siderophores, *Nat. Prod. Rep.*, 27, 637–657,
778 <https://doi.org/10.1039/b906679a>, 2010.

779 Hoffman, C. L., Nicholas, S. L., Ohnemus, D. C., Fitzsimmons, J. N., Sherrell, R. M., German, C. R., Heller,
780 M. I., Lee, J. mi, Lam, P. J., and Toner, B. M.: Near field iron and carbon chemistry of non buoyant
781 hydrothermal plume particles, Southern East Pacific Rise 15°S, *Mar. Chem.*, 201, 183–197,
782 <https://doi.org/10.1016/j.marchem.2018.01.011>, 2018.

783 Hoffman, C. L., Schladweiler, C., Seaton, N. C. A., Nicholas, S. L., Fitzsimmons, J., Sherrell, R. M., German,
784 C. R., Lam, P., and Toner, B. M.: Diagnostic morphology and solid state chemical speciation of
785 hydrothermally derived particulate Fe in a long range dispersing plume, *ACS Earth Sp. Chem.*, 4, 1831–
786 1842, <https://doi.org/10.1021/acsearthspacechem.0c00067>, 2020.

787 Homann, V. V., Sandy, M., Tineu, J. A., Templeton, A. S., Tebo, B. M., and Butler, A.: Loihichelins A–F,
788 a Suite of Amphiphilic Siderophores Produced by the Marine Bacterium *Halomonas* LOB-5, *J. Nat. Prod.*,
789 72, 884–888, 2009.

790 Kato, C. and Nogi, Y.: Correlation between phylogenetic structure and function : examples from deep sea
791 *Shewanella*, 35, 223–230, 2001.

792 Kelley, D. S. and Shank, T. M.: Hydrothermal systems: A decade of discovery in slow spreading
793 environments, *Geophys. Monogr. Ser.*, 188, 369–407, <https://doi.org/10.1029/2010GM000945>, 2010.

794 Kulmer, W. and Ingalls, A. E.: The R Journal: Tidy Data Neatly Resolves Mass Spectrometry’s Ragged
795 Arrays, *R J.*, 2022.

796 Lauderdale, J. M., Braakman, R., Forget, G., Dutkiewicz, S., and Follows, M. J.: Microbial feedbacks
797 optimize ocean iron availability, *Proc. Natl. Acad. Sci. U. S. A.*, 117, 4842–4849,
798 <https://doi.org/10.1073/pnas.1917277117>, 2020.

799 Li, M., Toner, B. M., Baker, B. J., Breier, J. a, Sheik, C. S., and Dick, G. J.: Microbial iron uptake as a
800 mechanism for dispersing iron from deep sea hydrothermal vents., *Nat. Commun.*, 5, 3192,
801 <https://doi.org/10.1038/ncomms4192>, 2014.

802 Lough, A. J. M., Tagliabue, A., Demasy, C., Resing, J. A., Mellett, T., Wyatt, N. J., and Lohan, M. C.: The
803 impact of hydrothermal vent geochemistry on the addition of iron to the deep ocean, *Biogeosciences Discuss.*,
804 [preprint], 1–23, <https://doi.org/10.5194/bg-2022-73>, 2022.

805 Manek, L. E., Park, J., Tully, B. J., Poire, A. M., Bundy, R. M., Dupont, C. L., and Barbeau, K. A.:

806 ~~Petrobactin, a siderophore produced by *Alteromonas*, mediates community iron acquisition in the global~~
807 ~~ocean, *ISME J.*, 16, 358–369, <https://doi.org/10.1038/s41396-021-01065-y>, 2022.~~

808 ~~Martinez, J. S., Carter Franklin, J. N., Mann, E. L., Martin, J. D., Haygood, M. G., and Butler, A.: Structure~~
809 ~~and membrane affinity of a suite of amphiphilic siderophores produced by a marine bacterium, *Proc. Natl.*~~
810 ~~*Acad. Sci. U. S. A.*, 100, 3754–3759, <https://doi.org/10.1073/pnas.0637444100>, 2003.~~

811 ~~Mellett, T., Albers, J. B., Santoro, A., Wang, W., Salaun, P., Resing, J., Lough, A. J., Tagliabue, A., Lohan,~~
812 ~~M., Bundy, R. M., and Buck, K. N.: Particle exchange mediated by organic ligands in incubation experiments~~
813 ~~of hydrothermal vent plumes along the mid-Atlantic Ridge, n.d.~~

814 ~~Moore, L. E., Heller, M. I., Barbeau, K. A., Moffett, J. W., and Bundy, R. M.: Organic complexation of iron~~
815 ~~by strong ligands and siderophores in the eastern tropical North Pacific oxygen deficient zone, *Mar. Chem.*,~~
816 ~~236, 104021, <https://doi.org/10.1016/j.marchem.2021.104021>, 2021.~~

817 ~~Omanović, D., Garnier, C., and Pižeta, I.: ProMCC: An all-in-one tool for trace metal complexation studies,~~
818 ~~*Mar. Chem.*, 173, 25–39, <https://doi.org/10.1016/j.marchem.2014.10.011>, 2015.~~

819 ~~Parada, A. E., Needham, D. M., and Fuhrman, J. A.: Every base matters: Assessing small subunit rRNA~~
820 ~~primers for marine microbiomes with mock communities, time series and global field samples, *Environ.*~~
821 ~~*Microbiol.*, 18, 1403–1414, <https://doi.org/10.1111/1462-2920.13023>, 2016.~~

822 ~~Park, J., Durham, B. P., Key, R. S., Groussman, R. D., Pinedo-Gonzalez, P., Hawco, N. J., John, S. G.,~~
823 ~~Carlson, M. C. G., Lindell, D., Juranek, L., Ferrón, S., Ribalet, F., Armbrust, E. V., Ingalls, A. E., and Bundy,~~
824 ~~R. M.: Siderophore production and utilization by microbes in the North Pacific Ocean, *bioRxiv*,~~
825 ~~2022.02.26.482025, <https://doi.org/10.1101/2022.02.26.482025>, 2022.~~

826 ~~Park, J., Durham, B. P., Key, R. S., Groussman, R. D., Pinedo-Gonzalez, P., Hawco, N. J., John, S. G.,~~
827 ~~Carlson, M. C. G., Lindell, D., Juranek, L., Ferrón, S., Ribalet, F., Armbrust, E. V., Ingalls, A. E., and Bundy,~~
828 ~~R. M.: Siderophore production and utilization by microbes in the North Pacific Ocean, *Limnol. Oceanogr.*,~~
829 ~~2022.02.26.482025, <https://doi.org/10.1002/lno.12373>, 2023.~~

830 ~~Quast, C., Pruesse, E., Yilmaz, P., Gerken, J., Schweer, T., Yarza, P., Peplies, J., and Glöckner, F. O.: The~~
831 ~~SILVA ribosomal RNA gene database project: Improved data processing and web-based tools, *Nucleic Acids*~~
832 ~~*Res.*, 41, 590–596, <https://doi.org/10.1093/nar/gks1219>, 2013.~~

833 ~~Resing, J. a., Sedwick, P. N., German, C. R., Jenkins, W. J., Moffett, J. W., Sohst, B. M., and Tagliabue, A.:~~
834 ~~Basin-scale transport of hydrothermal dissolved metals across the South Pacific Ocean, *Nature*, 523, 200–~~
835 ~~203, <https://doi.org/10.1038/nature14577>, 2015.~~

836 ~~Ruttkies, C., Schymanski, E. L., Wolf, S., Hollender, J., and Neumann, S.: MetFrag relaunched: incorporating~~
837 ~~strategies beyond in-silico fragmentation, *J. Cheminform.*, 8, 1–16, [https://doi.org/10.1186/s13321-016-](https://doi.org/10.1186/s13321-016-0115-9)~~
838 ~~0115-9, 2016.~~

839 ~~Sander, S. G. and Koschinsky, A.: Metal flux from hydrothermal vents increased by organic complexation,~~
840 ~~*Nat. Geosci.*, 4, 145–150, <https://doi.org/10.1038/ngeo1088>, 2011.~~

841 ~~Sandy, M. and Butler, A.: Microbial iron acquisition: marine and terrestrial siderophores., *Chem. Rev.*, 109,~~
842 ~~4580–95, <https://doi.org/10.1021/cr9002787>, 2009.~~

843 ~~Santoro, A. E., Casciotti, K. L., and Francis, C. A.: Activity, abundance and diversity of nitrifying archaea~~
844 ~~and bacteria in the central California Current, *Environ. Microbiol.*, 12, 1989–2006,~~
845 ~~<https://doi.org/10.1111/j.1462-2920.2010.02205.x>, 2010.~~

846 ~~Sorokina, M., Merseburger, P., Rajan, K., Yirik, M. A., and Steinbeck, C.: COCONUT-online: Collection of~~
847 ~~Open Natural Products database, *J. Cheminform.*, 13, 1–13, <https://doi.org/10.1186/s13321-020-00478-9>,~~
848 ~~2021.~~

849 Stephens, B. M., Opalk, K., Petras, D., Liu, S., Comstock, J., Aluwihare, L. I., Hansell, D. A., and Carlson,
850 C. A.: Organic Matter Composition at Ocean Station Papa Affects Its Bioavailability, Bacterioplankton
851 Growth Efficiency and the Responding Taxa, *Front. Mar. Sci.*, 7, <https://doi.org/10.3389/fmars.2020.590273>,
852 2020.

853 Sumner, L. W., Amberg, A., Barrett, D., Beale, M. H., Beger, R., Daykin, C. A., Fan, T. W. M., Fiehn, O.,
854 Goodacre, R., Griffin, J. L., Hankemeier, T., Hardy, N., Harnly, J., Higashi, R., Kopka, J., Lane, A. N.,
855 Lindon, J. C., Marriott, P., Nicholls, A. W., Reily, M. D., Thaden, J. J., and Viant, M. R.: Proposed minimum
856 reporting standards for chemical analysis, *Metabolomics*, 3, 211–221, <https://doi.org/10.1007/s11306-007-0082-2>, 2007.

858 Tagliabue, A., Bowie, A. R., Boyd, P. W., Buck, K. N., Johnson, K. S., and Saito, M. A.: The integral role
859 of iron in ocean biogeochemistry, *Nature*, 543, 51–59, <https://doi.org/10.1038/nature21058>, 2017.

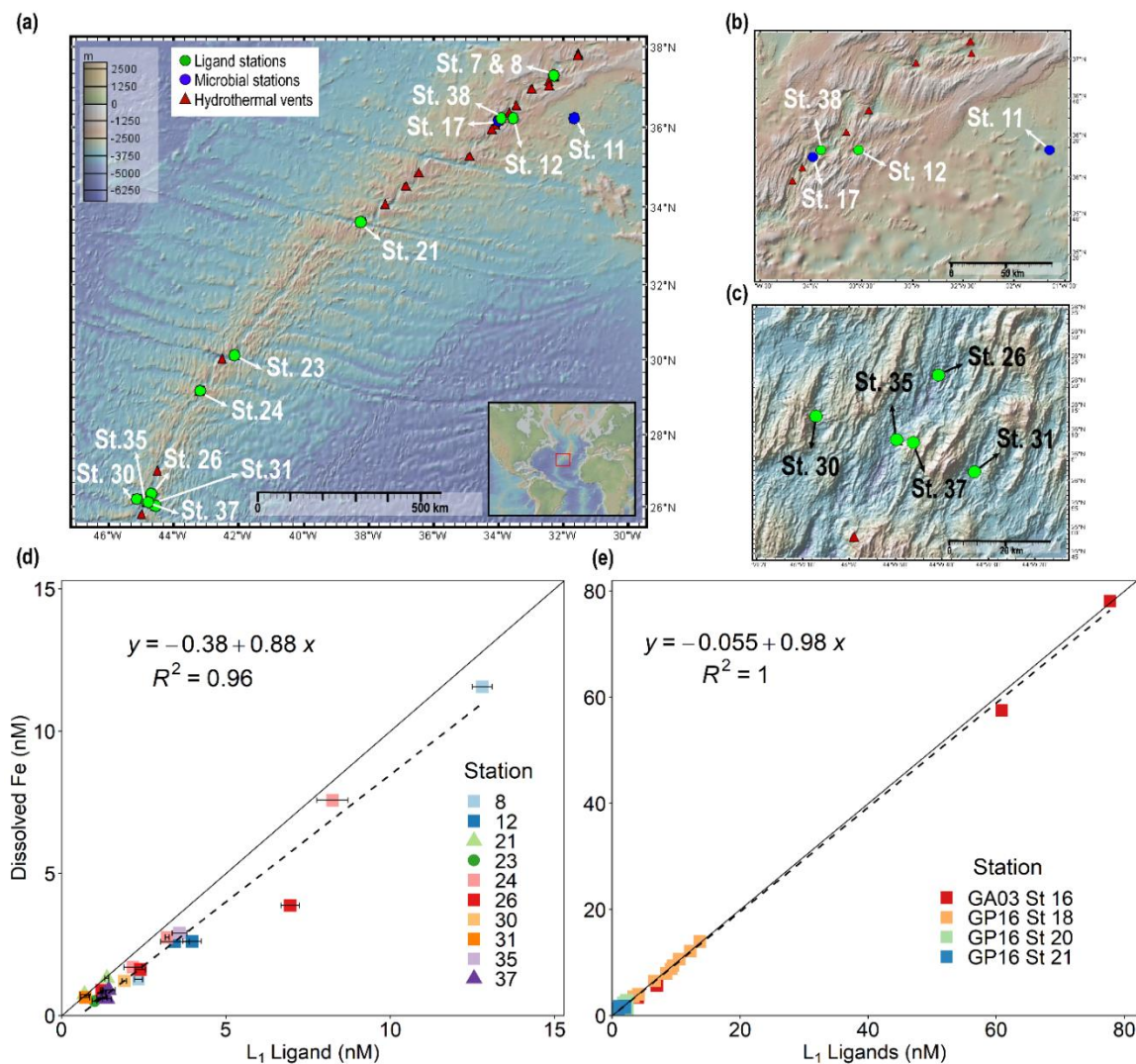
860 Toner, B. M., Fakra, S. C., Manganini, S. J., Santelli, C. M., Marcus, M. a., Moffett, J. W., Rouxel, O.,
861 German, C. R., and Edwards, K. J.: Preservation of iron(II) by carbon-rich matrices in a hydrothermal plume,
862 *Nat. Geosci.*, 2, 197–201, <https://doi.org/10.1038/ngeo433>, 2009.

863 Tortell, P. D., Maldonado, M. T., and Price, N. M.: The role of heterotrophic bacteria in iron-limited ocean
864 ecosystems, *Nature*, 383, 330–332, <https://doi.org/10.1038/383330a0>, 1996.

865 Vraspir, J. M. and Butler, A.: Chemistry of marine ligands and siderophores., *Ann. Rev. Mar. Sci.*, 1, 43–63,
866 <https://doi.org/10.1146/annurev.marine.010908.163712>, 2009.

867 Waska, H., Koschinsky, A., Ruiz Chanco, M. J., and Dittmar, T.: Investigating the potential of solid-phase
868 extraction and Fourier transform ion cyclotron resonance mass spectrometry (FT-ICR-MS) for the isolation
869 and identification of dissolved metal-organic complexes from natural waters, *Mar. Chem.*, 173, 78–92,
870 <https://doi.org/10.1016/j.marchem.2014.10.001>, 2015.

871



874

875 **Figure 1. Dissolved iron is strongly correlated with L₁ iron-binding ligands in diverse hydrothermal**876 **systems.** (a) Station map showing the 11 sites investigated along the MAR. Known hydrothermal vents are

877 marked as red triangles (Beaulieu and Szafranski, 2020). Two expanded inset maps for (b) Rainbow and (c)

878 TAG hydrothermal vent fields. For additional information about vent site characteristics refer to **Table 1**. (d)879 dFe versus L₁ iron-binding ligands at each vent site in this study showing a ~1:1 correlation ($m = 0.88$, $R^2 =$ 880 0.96) with dFe in neutrally-buoyant plumes along the MAR. (e) dFe versus L₁ ligands from previous studies

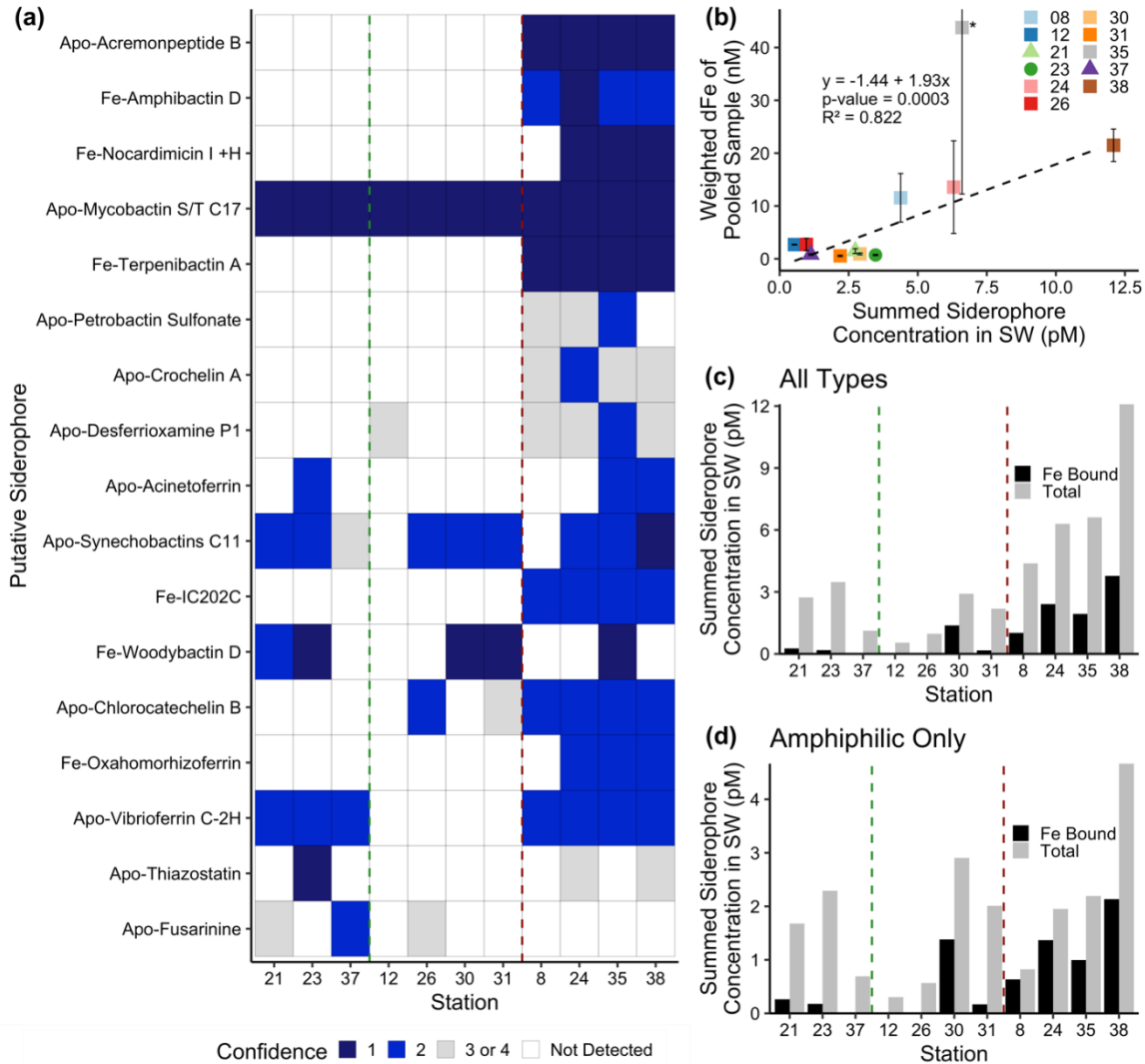
881 over the ridge axis and ~80 km from ridge axis in the Southern East Pacific Rise hydrothermal plume (Buck

882 et al., 2018), and over TAG hydrothermal vent field (Buck et al., 2015). The solid black lines in (d) and (e)

883 are the 1:1 ratio line between dFe and ligand concentrations, and dashed lines show the linear regression for

884 the corresponding data. Square symbols refer to spreading centers, triangles refer to fracture zones, and

885 circles refer to alkaline vents. Error bars represent the 95% confidence interval of the data fit as calculated
886 by ProMCC(Omanović et al., 2015). The map was created using GeoMapApp version 3.6.14.
887
888

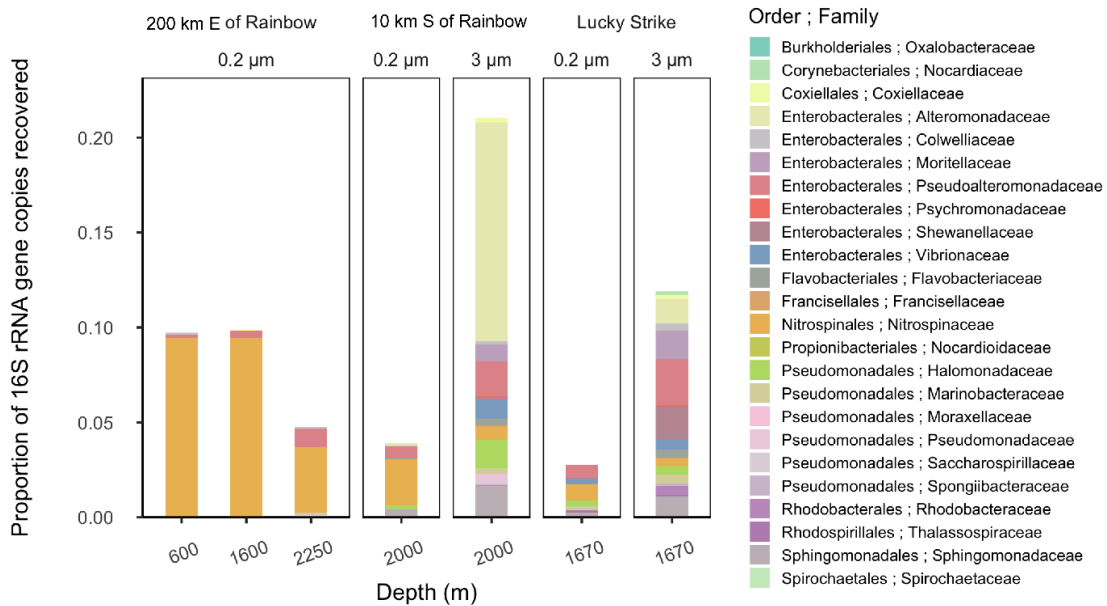


889

890

891 **Figure 2. Siderophore presence in hydrothermal plumes along the MAR.** (a) Heat map of confidence
 892 levels 1-2 (blue gradient, 1 = highest confidence). Gray boxes indicate a detection with lower confidence (see
 893 Methods), and white boxes indicate no detection at those sites. The y-axis is ordered from top to bottom in
 894 terms of descending mass of the apo (without Fe) form of the siderophore. (b) Model II ordinary least squares
 895 regression on dFe versus summed siderophore concentrations (of detections in Fig. 2b), calculated from peak
 896 areas, at each site. Since the siderophore analysis was performed on pooled samples, the dFe values in the
 897 regression are weighted values based on measured dFe and volume of each constituent of the pooled sample.
 898 The vertical error bars represent the standard deviation of dFe of the constituents. TAG (St. 35) — denoted
 899 by the asterisk — was not included in the regression due to its large range of dFe values and outlier behavior.
 900 (c-d) Fe bound versus total summed concentration of (c) all types of siderophores and (d) amphiphilic
 901 siderophores at each station. The vertical green lines separate fracture/diffuse sites from off-axis sites and
 902 vertical red lines separate off-axis from on-axis sites as defined in Table 1. Symbols follow Fig. 1.

903



904
 905
 906
 907
 908
 909
 910

Figure 3. Relative abundance of putative siderophore-producing taxa. Bar height indicates the proportion of 16S rRNA genes recovered in each sample, separated by depth from water surface, filter size fraction, and site location. Colors correspond to taxonomy. Genera found in MAR vent microbial communities with members in the antimash database predicted to produce siderophores are depicted at the family level.

Table 1. Characteristics of sample locations along the Mid Atlantic Ridge.

Vent Names	Abbr.	Station	Geology	Host rock	Vent type	Spreading rate (mm/yr)	Summed putative siderophore concentration (pM)	Summed Siderophore concentration/ L ₁ ligand (%)*
Lucky Strike	LS	7/8	Spreading Center	gabbro	Black smoker	20.2	4.38	0.034-0.19
33 km E of Rainbow	CER	12	Spreading Center	-	-	-	0.537	0.013-0.017
Rainbow	R	38	Spreading Center	ultramafic	Black smoker	20.6	12.1	<i>n.a.</i>
Hayes Fracture Zone	HFZ	21	Fracture Zone	peridotites/gabbro	-	21.2	2.74	0.20-0.39
Lost City	LC	23	Fracture Zone	ultramafic/gabbro	Alkaline	22.6	3.47	0.27-0.35
Broken Spur	BS	24	Spreading Center	gabbro	Black smoker/diffuse	22.9	6.30	0.07-0.29
29 km N of TAG	CNT	26	Spreading Center	-	-	-	0.968	0.014-0.079
30 km W of TAG	CWT	30	Spreading Center	-	-	-	2.91	0.15
30 km E of TAG	CET	31	Spreading Center	-	-	-	2.19	0.31

Trans-Atlantic Geotraverse	TAG	35	Spreading Center	gabbro	Black smoker	23.6	6.61	0.18
Low Temp Slope	LTS	37	-	-	Diffuse fluids	-	1.13	0.079-0.087

Spreading rates along the Mid-Atlantic Ridge were gathered from the Interridge Database v3.4. Host rock groups were determined from previously discussed classifications (Bazylev, 1997; Kelley and Shank, 2010). Off-axis sites –33 km E of Rainbow, 29 km N of TAG, 30 km E of TAG, and 30 km W of TAG– were far-field locations of their respective vent field. Low Temp Slope was a diffuse-dominated site that was sampled for the first time as a part of this study. Summed putative siderophore concentrations and the percent of L₁ ligand are reported for compounds detected with at least confidence level 1 and 2 at one site. These values do not take into account typical extraction efficiencies of ENV columns for Fe-binding organics. Average L₁ ligand and siderophore concentrations can be viewed in **Table S3** and concentrations for individual siderophores can be observed in **Table S5**.

*The siderophore sample at each site was pooled from ligand samples, so the percentage of siderophores in the L₁ pool is presented as a range based on the range of L₁ concentrations at each site.

n.a. = unable to be determined

- = unknown

